Molecular interactions of the physiological anti-hypertensive peptide catestatin with the neuronal nicotinic acetylcholine receptor

Bhavani S. Sahu[1,*], Jagan Mohan[1,*], Giriraj Sahu[1,*], Pradeep K. Singh[2], Parshuram J. Sonawane[1], Binu K. Sasi[1], Prasanna K. R. Allu[1], Samir K. Maji[2], Amal K. Bera[1,‡], Sanjib Senapati[1,‡] and Nitish R. Mahapatra[1,‡]

Department of Biotechnology, Bhupat and Jyoti Mehta School of Biosciences Building, Indian Institute of Technology Madras, Chennai 600036, India
Department of Biosciences and Bioengineering, Indian Institute of Technology Bombay, Powai, Mumbai 400076, India

*These authors contributed equally to this work
Authors for correspondence (amal@iitm.ac.in; sanjibs@iitm.ac.in; nmahapatra@iitm.ac.in)

Journal of Cell Science 125, 2787
2012. Published by The Company of Biologists Ltd
doi: 10.1242/jcs.114389

There was an error published in *J. Cell Sci.* **125**, 2323-2337.

The third corresponding author was inadvertently omitted from the title page.

All corresponding authors are now indicated above.

We apologise for this error.

Molecular interactions of the physiological anti-hypertensive peptide catestatin with the neuronal nicotinic acetylcholine receptor

Bhavani S. Sahu[1,*], Jagan M. Obbineni[1,*], Giriraj Sahu[1,*], Pradeep K. Singh[2], Parshuram J. Sonawane[1], Binu K. Sasi[1], Prasanna K. R. Allu[1], Samir K. Maji[2], Amal K. Bera[1,‡], Sanjib Senapati[1] and Nitish R. Mahapatra[1,‡]

[1]Department of Biotechnology, Bhupat and Jyoti Mehta School of Biosciences Building, Indian Institute of Technology Madras, Chennai 600036, India
[2]Department of Biosciences and Bioengineering, Indian Institute of Technology Bombay, Powai, Mumbai 400076, India

*These authors contributed equally to this work
‡Authors for correspondence (amal@iitm.ac.in; nmahapatra@iitm.ac.in)

Accepted 2 January 2012
Journal of Cell Science 125, 2323–2337

doi: 10.1242/jcs.103176

Summary

Catestatin (CST), a chromogranin-A-derived peptide, is a potent endogenous inhibitor of the neuronal nicotinic acetylcholine receptor (nAChR). It exerts an anti-hypertensive effect by acting as a 'physiological brake' on transmitter release into the circulation. However, the mechanism of interaction of CST with nAChR is only partially understood. To unravel molecular interactions of the wild-type human CST (CST-WT) as well as its naturally occurring variants (CST-364S and CST-370L, which have Gly→Ser and Pro→Leu substitutions, respectively) with the human α3β4 nAChR, we generated a homology-modeled human α3β4 nAChR structure and solution structures of CST peptides. Docking and molecular dynamics simulations showed that ~90% of interacting residues were within 15 N-terminal residues of CST peptides. The rank order of binding affinity of these peptides with nAChR was: CST-370L>CST-WT>CST-364S; the extent of occlusion of the receptor pore by these peptides was also in the same order. In corroboration with computational predictions, circular dichroism analysis revealed significant differences in global structures of CST peptides (e.g. the order of α-helical content was: CST-370L>CST-WT>CST-364S). Consistently, CST peptides blocked various stages of nAChR signal transduction, such as nicotine- or acetylcholine-evoked inward current, rise in intracellular Ca^{2+} and catecholamine secretion in or from neuron-differentiated PC12 cells, in the same rank order. Taken together, this study shows molecular interactions between human CST peptides and human α3β4 nAChR, and demonstrates that alterations in the CST secondary structure lead to the gain of potency for CST-370L and loss of potency for CST-364S. These findings have implications for understanding the nicotinic cholinergic signaling in humans.

Key words: Hypertension, Structure–function, nAChR, Catestatin, Human variation

Introduction

Catestatin (CST) is an endogenous 21 amino acid (human sequence: SSMKLSFRARAYGFRGPGPQL) peptide (Mahapatra, 2008; Mahata et al., 1997). It is generated from chromogranin A (CHGA) (Biswas et al., 2009; Helle, 2010), a major protein co-stored and co-released with catecholamines from secretory granules of chromaffin cells and adrenergic neurons (Sahu et al., 2010; Taupenot et al., 2003). Although CHGA is overexpressed in genetic hypertension (Friese et al., 2005; O'Connor et al., 1999; Takiyyuddin et al., 1995), the plasma CST level is diminished not only in established hypertensive patients but also in their normotensive offspring (O'Connor et al., 2002). Infusion of CST into dorsal hand veins triggers dose-dependent vasodilation in human subjects (Fung et al., 2010). Consistently, targeted ablation of the *CHGA* gene in mice leads to hypertension that can be rescued by administration of human CST (Mahapatra et al., 2005).

CST blocks nicotinic cholinergic-agonist-evoked exocytotic secretion from adrenal medullary chromaffin cells (Mahata et al., 2004) and cultured neurons (Rao et al., 2007). Interestingly, CST does not block the secretion caused by agents that raise intracellular Ca^{2+} without involving the neuronal nicotinic acetylcholine receptor [nAChR] (e.g. the calcium ionophore ionomycin; KCl, which opens voltage-gated Ca^{2+} channels; ATP, which acts on P2x receptors) (Mahapatra et al., 2006). Moreover, CST blocks nicotine-induced entry of extracellular Na^{+} into chromaffin cells, the initial step in the nicotinic cationic signal transduction (Mahata et al., 2004). These observations established CST as a specific antagonist at nAChRs, the physiological trigger to efferent autonomic outflow, and hence a regulator of catecholamine secretion into the circulation by a negative-feedback mechanism. We have also shown that any dose of nicotine cannot overcome the inhibition of catecholamine secretion by CST, suggesting the non-competitive nature of blockade of nAChRs by this peptide (Mahapatra, 2008; Mahata et al., 2004). However, the precise site at which CST interacts with nAChRs remains unknown.

While probing human genetic variations at the *CHGA* locus, we discovered two non-synonymous substitutions within the CST region: Gly364Ser and Pro370Leu (Wen et al., 2004); whereas 364Ser has not been detected in any other mammals, 370Leu is a reversion of the wild-type Pro residue to Leu residue seen in several non-primate mammals. Interestingly, the 364Ser variant

(CST-364S) is ~4.5-times less potent, whereas the 370Leu variant (CST-370L) is ~2.2-times more potent than the wild-type peptide (CST-WT) in inhibiting nicotine-evoked catecholamine release from PC12 cells (Mahapatra, 2008; Mahata et al., 2004). However, the molecular basis for such differential activities of these naturally occurring CST variants has not yet been investigated.

Here, we analyzed interactions of human CST peptides with the human α3β4 nAChR subtype, a major subtype expressed in chromaffin cells and adrenergic neurons harboring catecholamine-storage vesicles (Rezvani et al., 2010; Sala et al., 2008), by computational (docking and molecular dynamics simulations) as well as experimental (biochemical, biophysical, cell biology and electrophysiology) techniques. We observed molecular interactions between each human CST peptide and α3β4 nAChR, and demonstrated that alterations in the peptide secondary structure (especially, α-helical content) cause the gain of potency for CST-370L and loss of potency for CST-364S over CST-WT.

Results

Modeled structure of the human α3β4 nAChR

To study interactions of the human CST peptide with the human nAChR, an in silico model structure for the human α3β4 receptor subtype was developed by following a recently reported protocol for modeling the human α4β2 subtype (Haddadian et al., 2008). Accordingly, the available refined structure of the electric ray *Torpedo marmorata* $(\alpha)_2\beta\gamma\delta$ nAChR (PDB ID: 2BG9) was used as a template to build the pentameric human $(\alpha3)_2(\beta4)_3$ nAChR structure (Fig. 1A) by homology modeling. About 60% sequence similarity was found between the target (human α3 and β4) and template (*Torpedo* α and β) subunits sequences, ensuring a good starting point to model the human α3β4 receptor structure (supplementary material Fig. S1). Evaluation of the modeled human α3β4 nAChR structure revealed the absence of any residue in the strictly disallowed regions of the Ramachandran Plot (supplementary material Fig. S2). Superimposition of the modeled human $(\alpha3)_2(\beta4)_3$ nAChR structure with the *Torpedo* $(\alpha)_2\beta\gamma\delta$ nAChR structure showed excellent overlap of residues in the ligand binding extracellular (EC), transmembrane (TM) and intracellular (IC) domains of these receptors (Fig. 1B), suggesting that the model provides a reasonable representative of the human α3β4 receptor. The EC domain of the human α3β4 receptor was mainly constituted of β-strands (13 for each α3 subunit and 11 for each β4 subunit). Additionally, one α-helix was also present towards the N-terminus of both subunit types. The TM domain of the receptor was comprised of four TM helices from each of the subunits, and the IC domain was comprised of one helix from each of the subunits.

Because functional nAChRs require the presence of lipid and cholesterol molecules in the vicinity of the receptor molecules (Barrantes, 2004; Brannigan et al., 2008), the EC and TM domains of the modeled α3β4 nAChR structure (specifically, the M1, M2, M3 and M4 helices) were embedded in the equilibrated lipid bilayer (composed of POPC, POPA and cholesterol in the ratio of 3:1:1). The system was then equilibrated for 80 nanoseconds. Structural stability of the receptor in the bilayer (Fig. 1C) as assessed by evaluating the root-mean-square deviation (RMSD) of the Cα atoms of the receptor backbone was observed for 80 nanoseconds after the initial 10 nanoseconds (Fig. 1D). This bilayer-embedded receptor structure might serve as a useful model for docking with α3β4 nAChR agonists and antagonists for structure–function analysis studies.

Secondary and tertiary structures of the human CST peptides: computational predictions

To obtain the time-averaged structures of the wild type human catestatin (CST-WT) and that of the derived structures of CST-364S and CST-370L, the peptides were individually simulated for 180 nseconds in water with appropriate amounts of ions for charge neutralization. In general, although structures of all three CST peptides achieved stable conformations after the first 20 nanoseconds, they differed in the extent of fluctuations. The RMSD of C_α atoms in these three peptides as a function of time are shown in Fig. 2B. Clearly, the CST-WT structure was the most stable one, with a mean RMSD of 4.1Å from the starting structure (PDB ID: 1LV4). However, CST-364S structure showed ~twofold higher mean RMSD (8.5 Å), whereas the CST-370L structure displayed a relatively higher RMSD (5.5 Å) compared with the CST-WT.

The root-mean-square fluctuation (RMSF) values of the peptide structures are illustrated in Fig. 2C. The CST-WT and CST-370L structures displayed lower per residue RMSF than the CST-364S structure. Specifically, the leucine, serine, arginine and alanine residues at the 5th, 6th, 10th and 11th positions, respectively, in the CST-364S structure showed a high degree of fluctuation. Interestingly, the leucine residue at the 19th position of the CST-370L peptide showed insignificant fluctuation (with respect to the corresponding proline residue in the CST-WT), whereas the serine residue at the 13th position of the CST-364S peptide displayed ~fivefold higher fluctuation (than the corresponding glycine residue in the CST-WT). The first two N-terminal residues (SS) and the last two C-terminal residues (QL) showed very high fluctuations in all the three peptides, which are probably due to the intrinsic property of terminal residues in proteins or peptides to fluctuate.

Visualization of the molecular dynamics trajectories in visual molecular dynamics (VMDs) (Humphrey et al., 1996) revealed that the three peptides significantly differed among themselves in their propensities to adopt secondary structures in the following order: CST-370L>CST-WT>CST-364S. Specifically, considering the conformations during the relatively stable (with minimal fluctuations) 80 nanosecond time window of the simulation (from 40 nanoseconds to 120 nanoseconds), the percentage occurrence of secondary structures for these peptides was 73.4, 58.6 and 22.7 for CST-370L, CST-WT and CST-364S, respectively. In general, these peptides formed secondary structures comprising of a 3_{10} helix and an anti-parallel β-sheet. The representative secondary structures of these peptides are shown in Fig. 2D–F.

In the case of CST-WT, the arginine, alanine and tyrosine at the 10th, 11th and 12th positions contributed to a 3_{10} helix whereas the phenylalanine, arginine and alanine at the 7th, 8th and 9th positions, and the 14th to 18th residues (phenylalanine, arginine, glycine, proline and glycine) contributed to the anti-parallel β-sheet (Fig. 2D). By contrast, a completely different set of residues were involved in the CST-364S secondary structure formation: the 5th (leucine), 6th (serine) and 7th (phenylalanine) residues formed the 3_{10} helices; the 8th (arginine), 9th (alanine) and 12th to 15th residues (tyrosine, serine, phenyl alanine and arginine) formed the anti-parallel β-sheet (Fig. 2E). Interestingly, the residues involved in the secondary structure formation in the

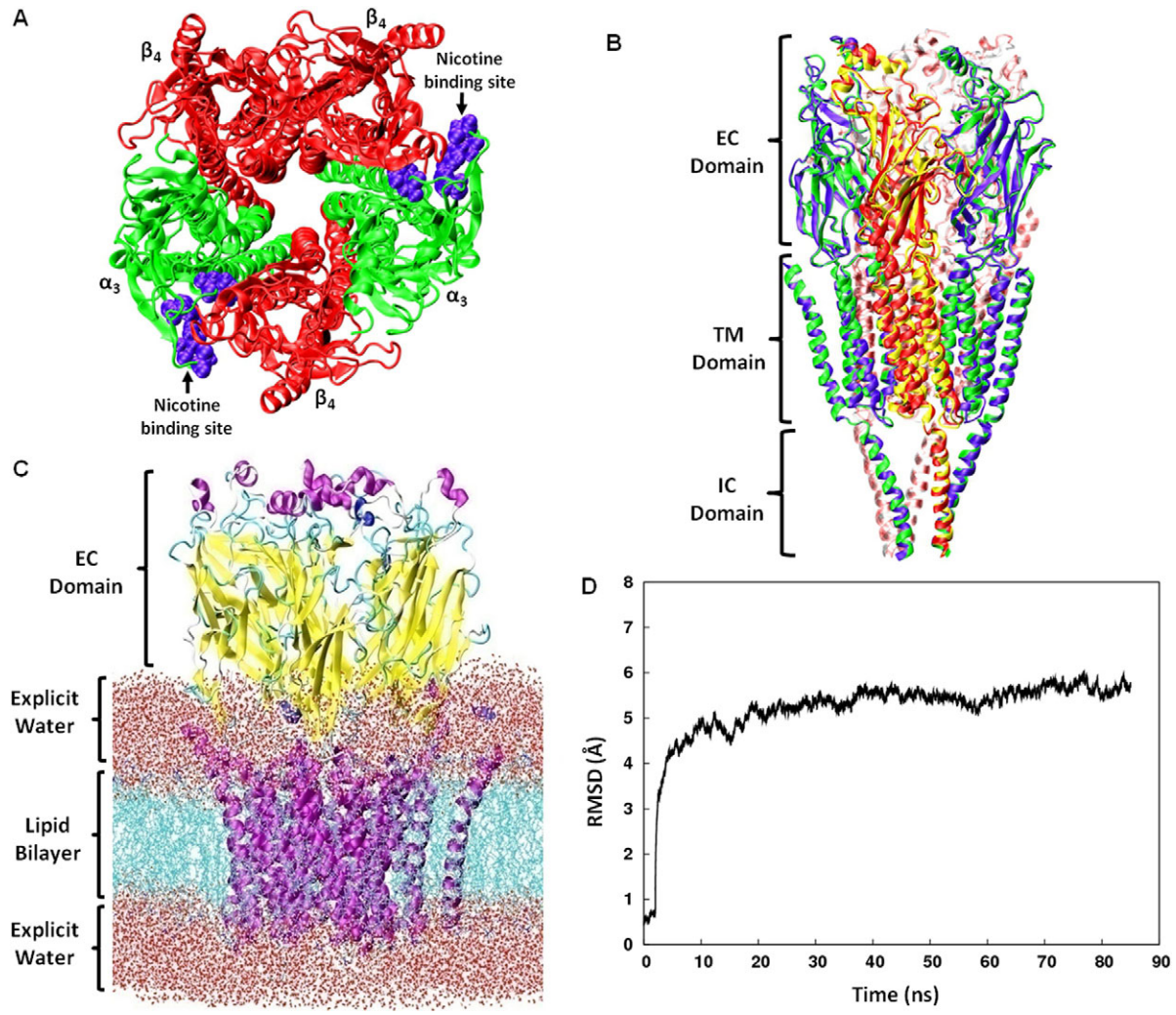

Fig. 1. Homology-modeled structure of the human α3β4 nicotinic acetylcholine receptor (nAChR). The α_3 and β_4 subunits of the modeled structure are shown in green and red, respectively. (**A**) Top view of the human α3β4 nAChR; the putative nicotine binding sites (based on the reported sites for the *Torpedo* nAChR and sequence alignment with human α3 subunit) are shown in deep purple and indicated by arrows. (**B**) Lateral view of the human α3β4 nAChR superimposed on to the *Torpedo marmorata* nAChR structure (PDB Id: 2GB9); among the five subunits (2α, β, γ, δ) of the *Torpedo* receptor, three frontal subunits [two α (light purple) and the γ (yellow)] are highlighted for clarity. The extracellular (EC), transmembrane (TM) and intracellular (IC) domains of the receptors are indicated. (**C**) Human α3β4 nAChR embedded in the lipid bilayer (POPC: POPA: cholesterol = 3:1:1) with explicit water; only the EC and TM domains are included (the IC domain was avoided to reduce computational cost); in the EC domain, water molecules were not shown for better visibility. (**D**) RMSD of Cα atoms for the human α3β4 nAChR as a function of time. The modeled structure attained stability after the initial 10 nanosecond molecular dynamics simulation.

case of CST-370L peptide are the same as those for CST-WT (Fig. 2F).

Experimental evidence for secondary structures of human CST peptides: Circular dichroism spectroscopic analysis

To verify our computational predictions (Fig. 2), we analyzed the secondary structure contents of the human CST peptides by circular dichroism (CD) spectroscopy in physiological buffer (PBS, pH 7.4). Deconvolution of the spectra (Fig. 3A,B,C) suggested the presence of significant amounts of secondary structures (α-helix plus β-sheet plus β-turn) in all three peptides: CST-WT (56%)>CST-364S (50%)>CST-370L (45%) (Fig. 3D). The β-sheets contributed most of the secondary structural contents; among these peptides, the percentage of β-sheets differed whereas the percentages of β-turns and α-helices were very similar (Fig. 3D).

To test whether hydrophobic environment (that occurs at lipid bilayers in the cell membranes) alters the extent of secondary structures, we carried out CD analysis with increasing percentages of 2,2,2-trifluoroethanol (TFE) in PBS. We chose TFE because there is a strong correlation between the TFE-induced structure and protein structure (Sönnichsen et al., 1992). A gradual increase in the global secondary structure (as reflected by the minima at 208 nm and 222 nm in the spectra; Fig. 3) was observed with increasing TFE concentration. Specifically, TFE provoked substantial α-helix formation in the cases of CST-370L and CST-WT, whereas the effect was significantly less in the case of the CST-364S peptide. For example, at 90% TFE, the α-helix content was: CST-370L (23%)>CST-WT (18%)>CST-364S (8%) (Fig. 3D). When comparing CST-370L and CST-WT, the propensity to assume α-helix conformation was higher for

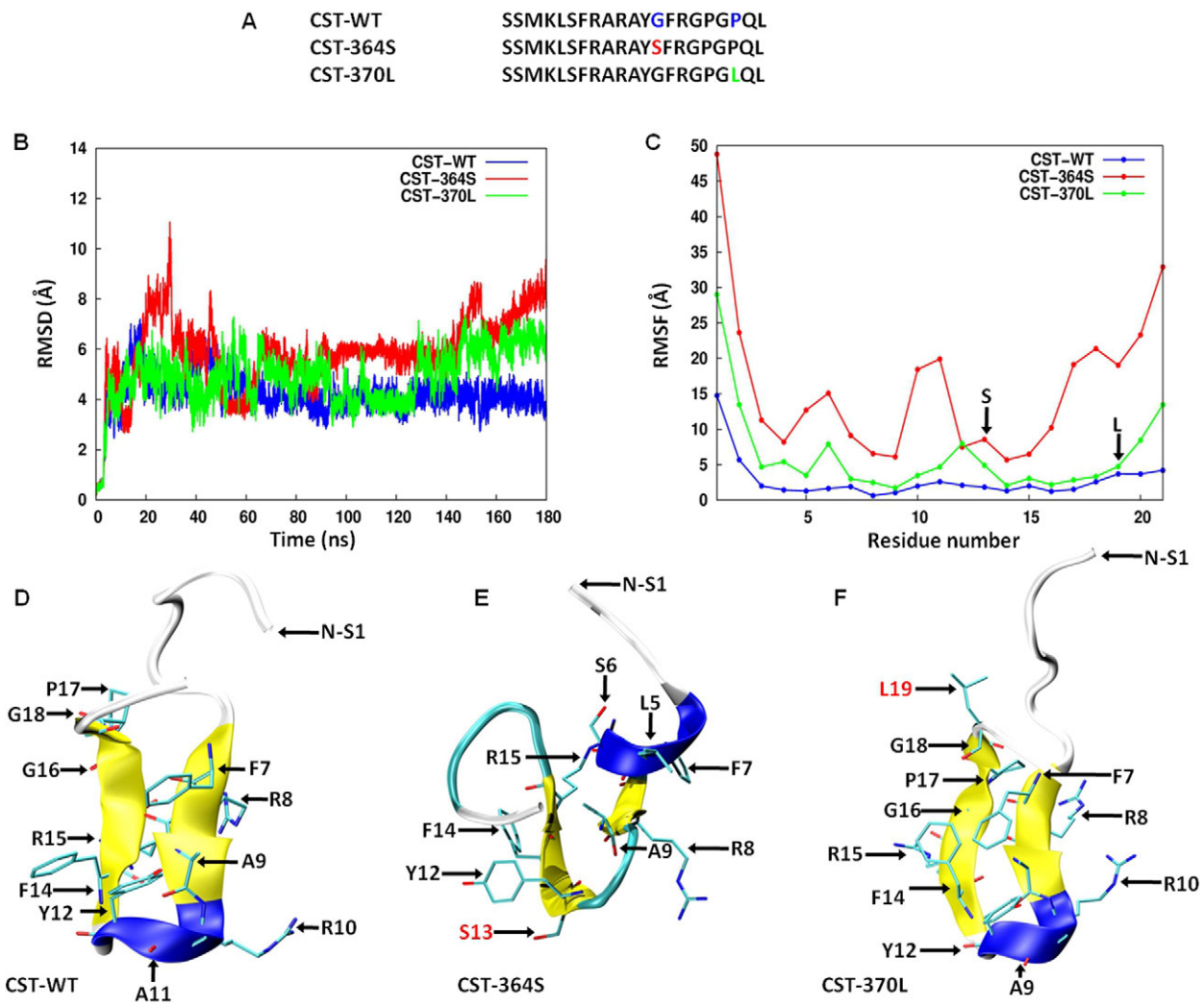

Fig. 2. Representative secondary structures of the human catestatin peptides. Equilibration and 170 nanosecond production-phase molecular dynamics simulation of solution, NMR structure of the human wild-type catestatin (CST-WT; PDB ID: 1LV4) and homology models of naturally occurring CST variants [CST-364S (substitution of Gly for Ser at the 13th position of the peptide that corresponds to the 364th position in the parent protein CHGA) and CST-370L (substitution of Pro for Leu at the 19th position of the peptide that corresponds to the 370th position in the parent protein CHGA)] revealed occurrence of conformations with secondary structures. (**A**) Primary amino acid sequence of CST-WT and variant peptides. The residues differing among these peptides are indicated in colored fonts. (**B**) RMSD of Cα atoms for the CST peptides as a function of time. (**C**) Root mean square fluctuations (RMSF) for the CST-peptides are shown as a function of residue number. The altered residues in case of the variant peptides are indicated by arrows. (**D**) Snapshot of a representative CST-WT conformation (having a 3_{10} helix and an anti-parallel β-sheet); 58.6% of conformations during the stable simulation period displayed secondary structural features. (**E**) Snapshot of a representative conformation of CST-364S with secondary structural features (having a 3_{10} helix and weak anti-parallel β-sheet); 22.7% of conformations during the stable simulation period displayed secondary structural features. The Ser13 residue is indicated by a red arrow. (**F**) Snapshot of a representative conformation (having a 3_{10} helix and an anti-parallel β-sheet) of CST-370L; 73.4% of conformations during the stable simulation period displayed secondary structural features. The Leu19 is indicated by a red arrow. The residues involved in the formation of secondary structures are shown in licorice representation.

CST-370L, which showed 21% helical content (compared with 8% for CST-WT) in the presence of 60% TFE (Fig. 3D).

Molecular interactions between human CST and human nAChR: docking and molecular dynamics simulations

To investigate likely molecular interactions between the human CST peptide and the human α3β4 nAChR, the CST-WT structure (Fig. 2D) was docked on to the receptor and the docked complex was simulated for about 80 nanoseconds to introduce flexibility in the receptor–ligand complex, so that a lower energy state can be reached. The CST-WT peptide-docked receptor was stable throughout the 80 nanosecond simulation period as evident from the C_α RMSD plot for the peptide (supplementary material Fig. S3). The positively charged amino acids of the peptide were observed to interact predominantly with the negatively charged amino acids in the A-loop of the receptor (Fig. 4A). Strong interactions of the positively charged residues of CST-WT (Lys4, Arg8, Arg10) with the negatively charged residues (Glu17 of the first α3 (designated α3-1) and Asp99, Asp103, Asp104 of the second α3 (α3-2) of the receptor suggested the crucial role of the charge-charge interactions for binding of the peptide to the receptor (Fig. 4A). Pi-Pi interaction between Phe7 of the peptide

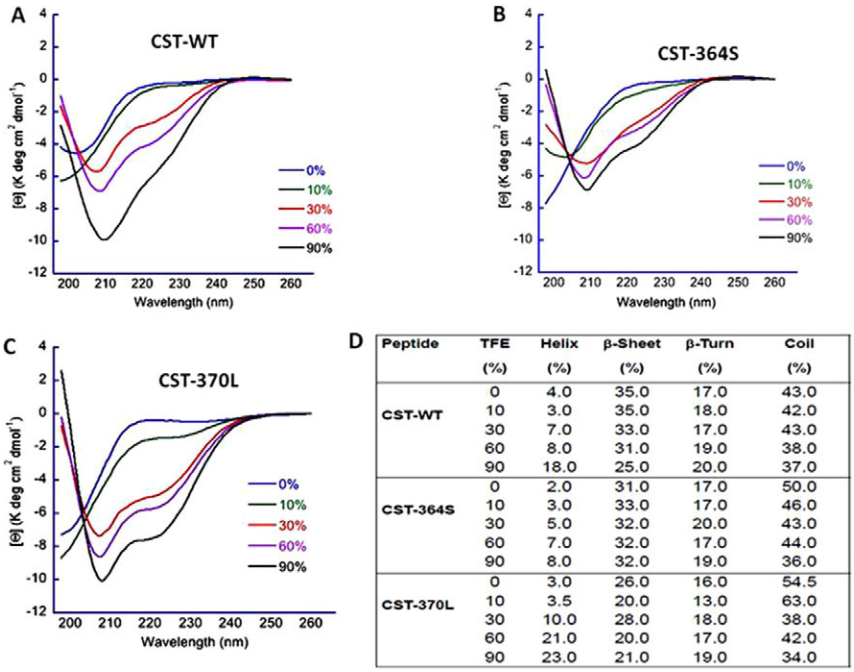

D

Peptide	TFE (%)	Helix (%)	β-Sheet (%)	β-Turn (%)	Coil (%)
CST-WT	0	4.0	35.0	17.0	43.0
	10	3.0	35.0	18.0	42.0
	30	7.0	33.0	17.0	43.0
	60	8.0	31.0	19.0	38.0
	90	18.0	25.0	20.0	37.0
CST-364S	0	2.0	31.0	17.0	50.0
	10	3.0	33.0	17.0	46.0
	30	5.0	32.0	20.0	43.0
	60	7.0	32.0	17.0	44.0
	90	8.0	32.0	19.0	36.0
CST-370L	0	3.0	26.0	16.0	54.5
	10	3.5	20.0	13.0	63.0
	30	10.0	28.0	18.0	38.0
	60	21.0	20.0	17.0	42.0
	90	23.0	21.0	19.0	34.0

Fig. 3. Circular dichroism spectra of CST peptides. CD spectra of the human CST peptides (at 100 μM concentration in PBS, pH 7.4) were monitored over 198–260 nm wavelength in the absence or presence of 10%, 30%, 60% and 90% trifluoroethanol (TFE). Increasing TFE concentration induced α-helix formation, as indicated by the two minima at 208 and 222 nm. The experiment was repeated three times and representative traces for CST-WT (**A**), CST-364S (**B**) and CST-370L (**C**) are shown. (**D**) The structural features (percentage of α-helix, β-turn, β-sheet and random coil) for the CST peptides at various TFE concentrations. The data were generated by deconvolution of spectra. The peptides displayed different propensities for formation of secondary structures (specifically, α-helix) in the following order: CST-370L>CST-WT>CST-364S.

with Tyr97 of the third β4 subunit (β4-3) of the receptor was also observed (Fig. 4A). Taken together, about 90% of the interacting residues of CST-WT were within the N-terminal 15 amino acids (Fig. 4B, top panel).

Similar analysis was carried to identify molecular interactions of CST-370L and CST-364S peptides with the nAChR. The CST-370L and CST-364S peptide–receptor complexes displayed stability during the entire simulation periods as evident from the C_α RMSD plots for the peptides (supplementary material Fig. S3). In the case of CST-364S, the Lys4, Arg8 and Arg15 residues were involved in the interactions with the Asp103, Asp104 of the α3-2 and Asp103 of the α3-1 subunits (Fig. 4B, bottom right). Intriguingly, in the case of CST-370L, the interactions of Arg8, Arg10 and Arg15 were confined to the Asp103, Asp104 of the α3-2 subunit (Fig. 4B, bottom left). In addition, a large number of hydrogen bonding and hydrophobic interactions were noted, as listed in Table 1.

Consistent with differential interactions of the CST peptides with the nAChR (the greater number of charge–charge interactions in the case of CST-370L compared with the other peptides), docking energy values for peptides were found to be in the following order: CST-370L (–21.83 kcal/mole)<CST-WT (–19.05 kcal/mole)<CST-364S (–13.17 kcal/mole).

Differential occlusions of the nAChR pore by human CST peptides

Inspection of the structures of the simulated CST-nAChR complexes revealed that CST peptides occlude the pore in the extracellular vestibule region of the receptor. To quantify the extent of occlusion of the pore of the human α3β4 nAChR, we carried out pore profile analysis by HOLE program (Smart et al., 1993). With respect to free nAChR, the percentage occlusion of the pore was in the following order: CST-370L (90%)>CST-WT (85%)>CST-364 (35%). Consequently, the minimum pore radius (MPR) for the extracellular vestibule region of the free nAChR (4.17 Å) dramatically decreased after the binding of CST-WT or CST-370L, whereas the effect was less pronounced in the case of CST-364S (Fig. 5A–D). Analysis of the pore profile for the average structures of the receptor–CST complexes also yielded approximately similar results; the MPR values were: CST-370L (0.436 Å)<CST-WT (0.631 Å)<CST-364S (2.768 Å) (Fig. 5E). Corroboratively, the predicted molar conductance values were in the following order: CST-370L (240 pS/M)<CST-WT (360 pS/M)<CST-364S (1300 pS/M).

Effect of human CST variants on blockade of acetylcholine-evoked currents

For verification of the computational prediction that the human CST-WT and its naturally occurring variants occlude the pore of the human α3β4 nAChR to different extents, we measured the inward current (I_{ACh}) after application of ACh onto voltage-clamped (at −80 mV) PC12 cells in the presence or absence of each CST peptide. The I_{ACh} was almost completely (~95%) blocked by d-Tubocurarine (25 μM), a specific nAChR inhibitor, confirming that the currents were generated by activation of nAChR channels (supplementary material Fig. S4). In these experiments, we used neuronally differentiated PC12 cells that predominantly express α3β4 nAChR subtype (Avila et al., 2003; Henderson et al., 1994) and gave larger and more reproducible amperometric responses to ACh as found by us and other investigators (Nery et al., 2010) compared with un-differentiated PC12 cells.

In one set of experiments, brief pulses (3 seconds) of ACh (100 μM) were applied to elicit I_{ACh} before, during and after application of CST peptides. Representative I_{ACh} traces for each CST peptide are shown in Fig. 6A–C. Two consecutive pulses of ACh separated by at least 2 minutes wash yielded I_{ACh} peaks of similar amplitudes (mean current=490±25 pA, n=51 cells; 1st and 2nd traces from the left in Fig. 6A–C). Each CST peptide significantly blocked I_{ACh} (the blocking effects at 2.5 μM dose are shown in 3rd trace in Fig. 6A–C); the extents of blockade of inward current by these peptides (i.e. efficacies of the peptides)

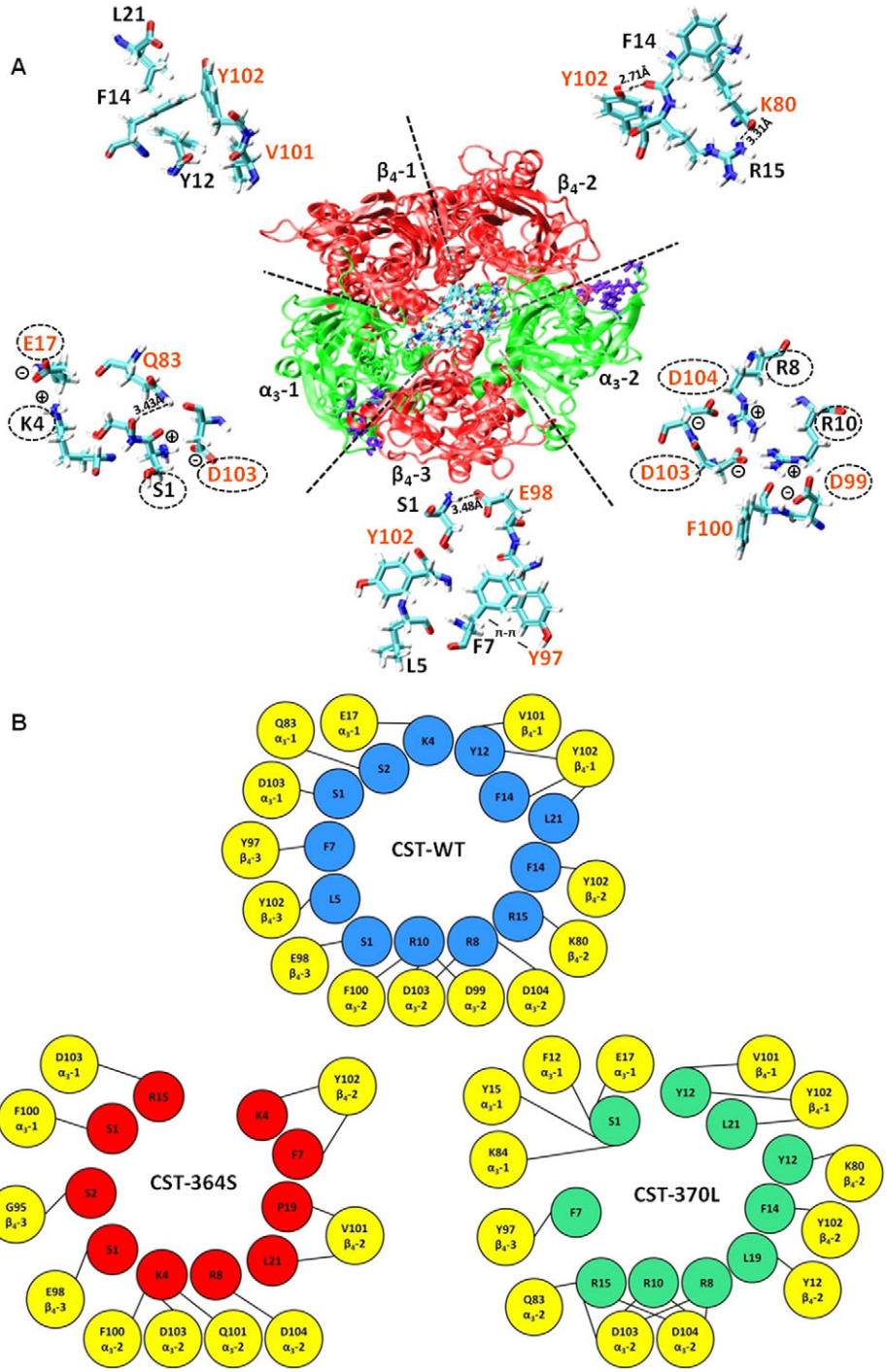

Fig. 4. Interaction of human CST peptides with the human $(\alpha3)_2(\beta4)_3$ nAChR. Docking of the CST peptides onto the α3β4 nAChR, followed by molecular dynamics simulations showed interacting residues of each peptide and the receptor. The various interactions for each of the three peptides are listed in Table 1. (**A**) The docked structure of the CST-WT on the receptor (viewed from the top) is shown, as an example. The two α3 subunits are shown in green whereas the three β4 subunits are shown in red; the CST-WT peptide is shown in licorice representation with conventional colors for various atoms and the putative nicotine binding sites are shown in purple. For each nAChR subunit, just outside the docked structure, the interacting residues are shown: peptide residues are labeled in black and receptor residues are labeled in orange. Charge–charge interactions are highlighted in dotted circles. (**B**) A schematic of the interacting residues of CST-WT (top), CST-364S (left) and CST-370L (right) peptides with the specific residues of the $(\alpha3)_2(\beta4)_3$ nAChR. The interactions are represented by connecting lines; the receptor residues are shown in yellow circles and their respective subunits are indicated.

at 10 μM dose were in the following order: CST-370L (81.9±1.5%)>CST-WT (68.0±1.8%)>CST-364S (55.4±1.3%). This observation is consistent with the rank order of inhibition of nicotine-induced $^{22}Na^{+}$ translocation into PC12 cells: CST-370L (~98%)>CST-WT (~87.0%)>CST-364S (~74%), as we reported previously (Mahata et al., 2004).

Interestingly, the blocking effect was reversible after washout of the peptide (4th trace in Fig. 6A–C). Of note, the CST peptides (at 5 μM) alone did not produce any current response and the magnitude of I_{ACh} blockade was much less when the peptides were co-applied with ACh without pre-incubation (data not shown). All three CST peptides blocked I_{ACh} in a concentration-dependent manner (Fig. 6D). However, the peptides displayed different potencies; IC_{50} values for CST blockade of I_{ACh} were in the following order: CST-370L (1.86 μM)<CST-WT (3.87 μM)<CST-364S (6.67 μM).

In another set of experiments, application of ACh was carried out for 40–60 seconds (until the peak I_{Ach} value reduced basal levels) to test whether the CST peptides modulate activation and desensitization kinetics of the nAChR. Representative traces (Fig. 7A–C) demonstrate that whereas the rate of activation were slower for CST-WT, the rates of desensitization were faster in the presence of all three peptides than ACh alone, indicating that

Table 1. Comparative interactions of human CST peptides* with the human α3β4 nAChR

nAChR subunit	Type of interaction	CST-WT	CST-364S	CST-370L
α3-1	Main-chain–main-chain hydrogen bonds	–	–	Phe12-**Ser1**, Tyr15-**Ser1**
	Main-chain–side-chain hydrogen bonds	Gln83-**Ser2**, Asp103-**Ser1**	Phe100-**Ser1**	Lys84-**Ser1**, Glu17-**Ser1**
	Ionic interactions	Glu17-**Lys4**	Asp103-**Arg15**	–
β4-1	Hydrophobic interactions	Val101-**Tyr12**, Tyr102-**Tyr12**, Tyr102-**Phe14**, Tyr102-**Leu21**	–	Val101-**Tyr12**, Tyr102-**Tyr12**, Tyr102-**Leu21**
β4-2	Main-chain–side-chain hydrogen bonds	Tyr102-**Phe14**, Lys80-**Arg15**	Tyr102-**Lys4**	Lys80-**Tyr12**
	Hydrophobic interactions	–	Val101-**Pro19**, Val101-**Leu21**, Tyr102-**Phe7**	Tyr102-**Phe14**, Tyr12-**Leu19**
α3-2	Main-chain–side-chain hydrogen bonds	Phe100-**Arg10**	Gln101-**Lys4**, Phe100-**Lys4**	Asp103-**Arg15**
	Side-chain–side-chain hydrogen bonds	Asp103-**Arg8**, Asp104-**Arg8**, Asp99-**Arg10**, Asp103-**Arg10**	Asp104-**Arg8**	Asp103-**Arg10**, Gln83-**Arg15**
	Ionic interactions	Asp99-**Arg10**, Asp103-**Arg10**, Asp103-**Arg8**, Asp104-**Arg8**	Asp104-**Arg8**, Asp103-**Lys4**	Asp103-**Arg15**, Asp103-**Arg10**, Asp103-**Arg8**, Asp104-**Arg15**, Asp104-**Arg10**, Asp104-**Arg8**
β4-3	Main-chain–side-chain hydrogen bonds	Glu98-**Ser1**	Glu98-**Ser1**, Gly95-**Ser2**	–
	Hydrophobic interactions	Tyr97-**Phe7**, Tyr102-**Leu5**	–	Tyr97-**Phe7**

*The specific residues of CST peptides involved in interactions are shown in bold.

these peptides, in general, blunted the nAChR function. Among the three peptides, the rate of activation of nAChR was significantly faster in the presence of CST-370L, as reflected by the significantly lower $\tau_{activation(CST)}$:$\tau_{activation(ACh)}$ ratio compared with the ratio for CST-WT (0.98±0.05 vs 1.41±0.09, P=0.011; Fig. 7D). In addition, the rate of nAChR desensitization was slower in the case of CST-364S, as reflected by the significantly higher $\tau_{desensitization(CST)}$:$\tau_{desensitization(ACh)}$ ratio, in comparison with CST-WT (0.38±0.08 vs 0.12±0.02, P=0.024; Fig. 7E).

Effect of human CST variants on intracellular Ca^{2+} concentration

Because the human CST peptides blocked the inward current elicited by ACh to different extents (Fig. 6), we hypothesized that intracellular free calcium concentration ($[Ca^{2+}]_i$) would also be modulated differently by these peptides. To test this hypothesis, neuronally differentiated PC12 cells were stimulated with two brief pulses (15–30 seconds) of nicotine followed by an incubation period of 2 minutes with a peptide. One CST peptide and nicotine were then co-applied that was followed by a recovery dose. The 1st and 2nd traces in Fig. 8A–C show the fast and transient increase of the $[Ca^{2+}]_i$ after nicotine. The basal and nicotine-stimulated $[Ca^{2+}]_i$ levels were 77±5 nM (n=49 cells) and 1072±53 nM (n=49 cells), respectively. Each CST peptide blocked the nicotine-stimulated $[Ca^{2+}]_i$ rise (Fig. 8A–C, 3rd trace); pre-incubation with the peptide was required to obtain a clear and significant effect on $[Ca^{2+}]_i$ signal. The extents of blockade of $[Ca^{2+}]_i$ rise (Fig. 8D) were different among the CST peptides: CST-370L (~65%)>CST-WT (~52%)>CST-364S (~42%). Interestingly, blocking effects were recovered upon re-stimulation of cells by nicotine, although to different extents (Fig. 8A–C, 4th trace); specifically, in the cases of CST-370L and CST-WT, the recovery was incomplete.

Differential inhibition of catecholamine secretion by CST peptides

To determine whether the human CST variants display differential efficacies in blocking catecholamine release from neuronally differentiated PC12 cells, we measured the exogenous norepinephrine secretion stimulated by nicotine in the presence or absence of each CST peptide. Consistent with the rank order of blockade of $[Ca^{2+}]_i$ rise (Fig. 8), the CST peptides blocked [^{3}H]norepinephrine secretion from NGF-differentiated PC12 cells in the following order: CST-370L (~76%)>CST-WT (~46%)>CST-364S (~19%) (Fig. 9A). In another set of experiments, we also assessed the efficacy of these peptides to block nicotine-evoked [^{3}H]norepinephrine secretion from undifferentiated PC12 cells, which displayed a similar effect (albeit, a relatively stronger response than in differentiated cells) and blocked [^{3}H]norepinephrine secretion in the same order: CST-370L (~94%)>CST-WT (~84%)>CST-364S (~37%) (Fig. 9B). In neuronally differentiated PC12 cells, the inhibitory effect of each CST peptide on nicotinic-cholinergic-induced catecholamine secretion (the final step of nicotinic signal transduction) correlated (correlation co-efficient, R=0.99; Fig. 9C) with the blockade of ACh-evoked inward current (the initial step of the signal transduction), reflecting the specific interaction of these peptides at nAChRs.

Discussion

Structure of the human α3β4 nAChR

Owing to the non-availability of high-resolution structures of any human nAChR subtype, mechanistic details of molecular interactions between the physiological anti-hypertensive peptide CST, a potent and specific inhibitor of nAChR (Mahapatra et al., 2006; Mahata et al., 1997), remained elusive. In this study, we generated a homology-modeled structure of the human α3β4 nAChR based on the *Torpedo* nAChR structure. To our knowledge, this is the first report of an all-atomic model of the human α3β4 nAChR (Fig. 1). The structure, embedded in lipid bilayer attained stability after 10 nanosecond molecular dynamics simulations. Previously, a homology model of the extracellular domain of the α3β4 nAChR was reported using the structure of ACh binding proteins from *Aplysia californica* and *Lymnaea stagnalis* (Rana et al., 2009); qualitative comparison of this model with the extracellular domain of our model showed similar locations for various residues in both structures. Of note,

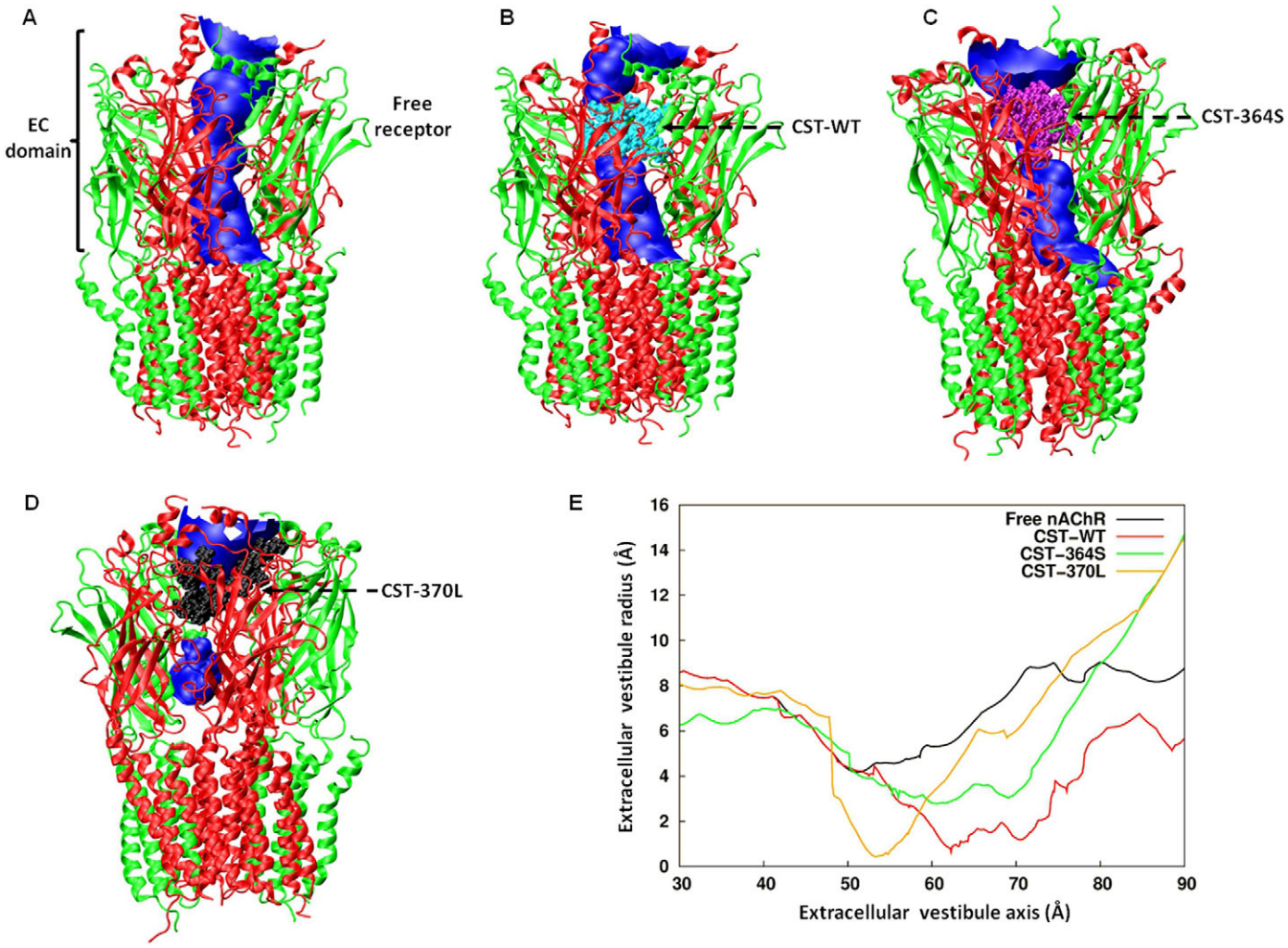

Fig. 5. Snapshots of the docked human CST peptides on the human nAChR. The peptides were docked on to the α3β4 nAChR, followed by MD simulation as described in the Materials and Methods. Pore profiles of the extracellular vestibule were analyzed using the Hole program (Smart et al., 1993). The extracellular and transmembrane domains were taken for this analysis; and the profiling was done only for the extracellular vestibule region. (**A**) Free unbound human α3β4 nAChR. (**B**) CST-WT (shown in cyan) docked on to human α3β4 nAChR. (**C**) CST-364S (shown in magenta) docked on to human α3β4 nAChR. (**D**) CST-370L (shown in black) docked on to nAChR. In A–D, the blue cylinder traversing through the EC domain indicates the accessible pore of the receptor. (**E**) Plot of the extracellular vestibule axis (Å) as a function of extracellular vestibule radius (Å) deciphering the extent of extracellular vestibule occlusion by the peptides. The traces are color-coded as follows: free nAChR, black; CST-WT, red; CST-364S, green; and CST-370L, orange. The minimum pore radius (MPR) of the extracellular vestibule for free nAChR was about 4.17 Å, which dramatically decreased after peptide binding. The MPR were in the following order: CST-370L (0.436 Å)<CST-WT (0.631 Å)<CST-364S (2.768 Å).

the conformation of the C-loop is open in the α-subunits and closed in the β-subunits of our modeled human α3β4 nAChR. This observation is similar to the conformations (in the corresponding subunits) in the X-ray structure of the *Torpedo* nAChR (Unwin, 2005), the modeled structure of the human α4β2 nAChR (Haddadian et al., 2008) and the modeled structure of the human α7 nAChR (Brannigan et al., 2008; Law et al., 2005).

Secondary structures of human CST peptides

Our previous analysis of the human CST peptide (CST-WT) structure by NMR suggested a loosely coiled structure (PDB ID: 1LV4) and the absence of secondary structural features (such as α-helices or β-sheets) in solution (Preece et al., 2004). However, another study modeling the bovine CST peptide (PDB ID: 1cfk) suggested a β-strand–loop–β-strand active conformation secured by hydrophobic interactions (Tsigelny et al., 1998). In the present study, extensive molecular dynamics simulation of the NMR-resolved structure (PDB ID: 1LV4) predicted the presence of several low-energy-state conformations that harbor significant amount of secondary structures (comprising of a 3_{10} helix and an anti-parallel β-sheet) in the CST-WT peptide (Fig. 2D). The extent of occurrence of these secondary structural features was higher for CST-370L (which contains a Leu residue instead of a Pro residue, a typical 'helix-breaker') and lower for the CST-364S (which contains a serine residue instead of glycine) than for CST-WT (Fig. 2E,F). These predictions for secondary structures for CST peptides agree well with our CD analysis results, showing differential α-helical and β-sheet contents for these peptides (Fig. 3D).

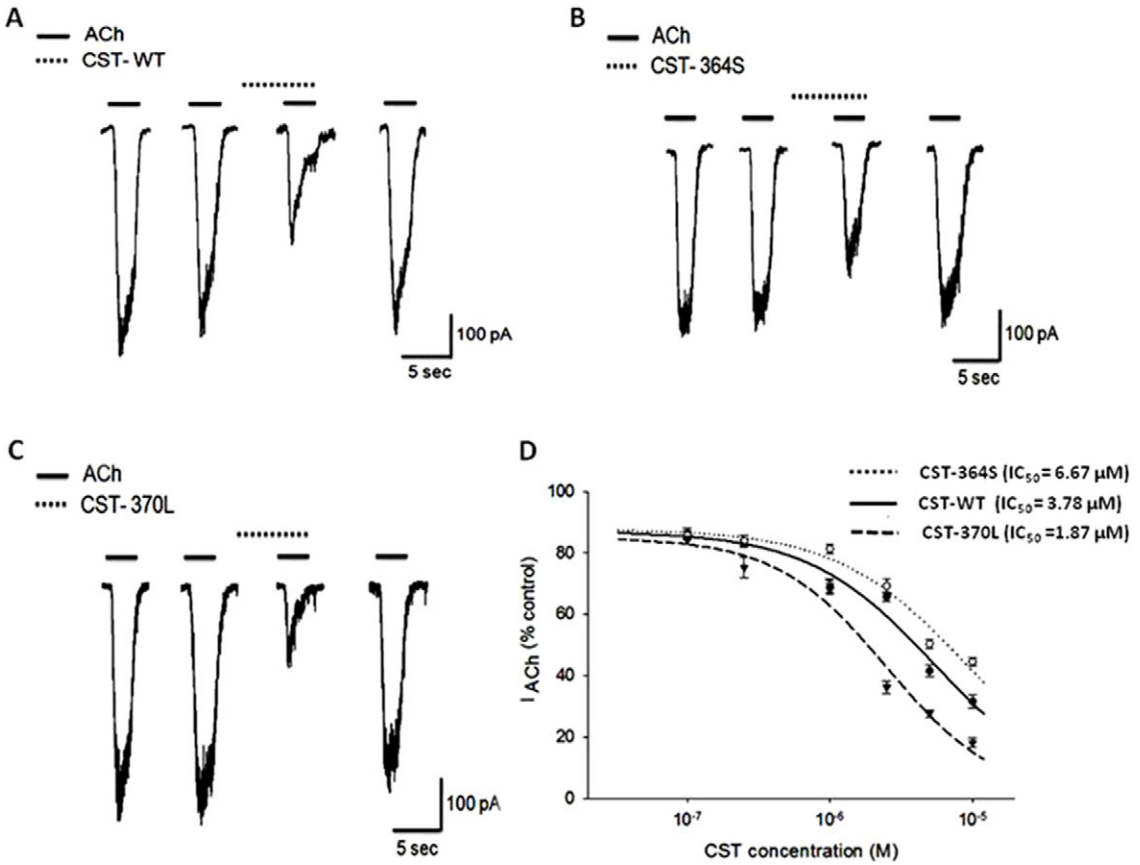

Fig. 6. Human CST peptides inhibit acetylcholine-evoked inward current in PC12 cells. NGF-differentiated PC12 cells, voltage-clamped at −80 mV, were stimulated with brief pulses (3 seconds) of ACh (100 μM) in the absence or presence of CST peptides. (**A**–**C**) Representative traces for inhibition of inward current (I_{ACh}) by 2.5 μM of CST-WT, CST-364S and CST-370L, respectively. The solid bars above the traces indicate the applications of ACh and the dotted bars indicate the application of peptides in these experiments. (**D**) Dose-response curves for inhibition of inward currents by CST peptides. Values are expressed as a percentage of control I_{ACh} (in the absence of peptides), measured at the peak amplitude. Each point in the curves represents mean ± s.e.m. of values obtained from 6–7 cells. IC_{50} values were determined by non-linear regression wizard with three-parameter logistic equation; the co-efficient of correlation in case of each peptide was 0.98.

A recent study analyzed the structures of CST peptides in the presence of dodecylphosphocholine (DPC) micelles and phospholipid bilayers (to mimic interfacial properties of cell membranes) by CD and NMR spectroscopy; these peptides displayed ≥20±5% of α-helix in the following order: CST-370L>CST-WT∼CST-364S (Sugawara et al., 2010). Clearly, these reported helical contents for CST peptides in the presence of DPC match well with our CD analysis in TFE (Fig. 3D). In addition, the CD and NMR data for these peptides (Sugawara et al., 2010) suggested that the helix extended from residues 7 to 11 (Phe7, Arg8, Ala9, Arg10 and Ala11), with additional medium range contacts involving Ser6 and Tyr12. This is in good agreement with our computational prediction that Arg10, Ala11 and Tyr12 residues contributed to a 3_{10} helix in the case of CST-WT and CST-370L whereas Leu5, Ser6 and Phe7 residues formed the 3_{10} helix in the case of CST-364S (Fig. 2D,E,F). Interestingly, the crucial residues for the nicotine-evoked inhibition of catecholamine release in the bovine ortholog of the human CST peptide included Leu5, Phe7, Arg8, Arg10, Gly11 and Tyr12 (Mahata et al., 2000). Because the corresponding residues (with respect to the bovine CST) in the human CST peptides are involved in α-helix formation (this study) (Sugawara et al., 2010), it appears that the functional activity of CST peptides across species is governed by their helical content.

Mechanism of interaction of the human CST-WT with the human α3β4 nAChR

The docking of CST-WT on the nAChR revealed that the peptide strongly interacted with specific residues in the extracellular domains of two α3 subunits, distinctly away from the nicotine binding sites (Fig. 4 and Table 1) and occluded as much as 85% of the pore in the receptor vestibule (Fig. 5B). This observation provides a structural basis for the non-competitive antagonistic function of CST at nAChRs. Our computational analysis further predicted that about 90% of the interacting residues were within the 15 N-terminal amino acids of the peptide, consistent with the experimental results from alanine-scan experiments for the bovine CST peptide (which has 80.9% homology with the CST-WT sequence) (Mahata et al., 2000).

Notably, our electrophysiology and calcium imaging experiments on adrenal chromaffin PC12 cells showed that pre-incubation with the human CST-WT peptide produced a greater inhibition of the peak current (I_{ACh}) and $[Ca^{2+}]_i$ rise responses than its co-application with nicotinic cholinergic agonists,

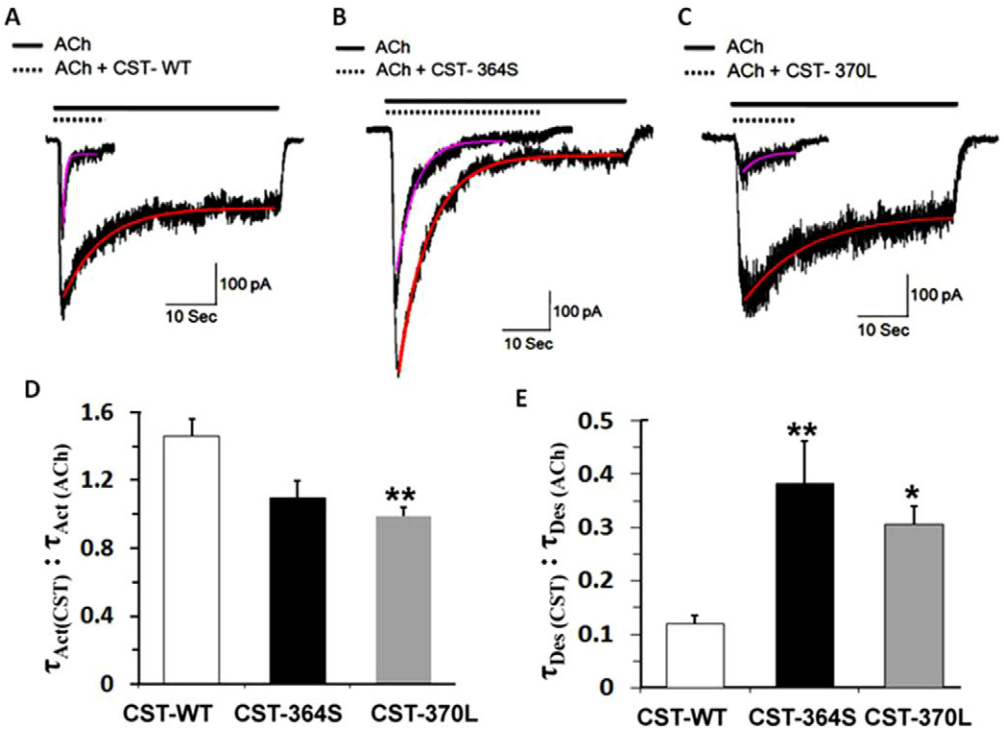

Fig. 7. Effect of human CST peptides on the rate of activation or desensitization of nAChR. Inward currents (I_{ACh}) were measured in NGF-differentiated-PC12 cells upon application of ACh (100 μM) for 40–60 seconds in the presence or absence of CST peptides (5 μM). (**A–C**) Representative I_{ACh} traces for CST-WT, CST-364S and CST-360L, respectively. (**D**) Comparison of peptide-modulated nAChR activation kinetics among the CST peptides. The $\tau_{activation(CST)}$: $\tau_{activation(ACh)}$ was calculated from I_{ACh} traces (e.g. those shown in A–C) in the case of each peptide. The mean ± s.e. of this ratio for a number of cells (n=8 for CST-WT, n=5 for CST-364S and n=7 for CST-370L) were plotted for each peptide. The activation kinetics was significantly different among the peptides as determined by one-way ANOVA with multiple-comparison post-hoc tests (ANOVA F=7.54, P<0.01). Specifically, CST-370L caused ~1.4-fold faster activation of the receptor than CST-WT. *P<0.05 with respect to CST-WT. The activation kinetics among the other groups (CST-WT vs CST-364S and CST-364S vs CST-370L) did not differ significantly. (**E**) Comparison of peptide-modulated nAChR desensitization kinetics among the CST peptides. The $\tau_{desensitization\ (CST)}$: $\tau_{\ desensitization\ (ACh)}$ was calculated from I_{ACh} traces in the case of each peptide. The mean ± s.e. of this ratio for a number of cells (n=7 for CST-WT, n=5 for CST-364S and n=7 for CST-370L) were plotted for each peptide. The desensitization kinetics was significantly different between the peptides as determined by one-way ANOVA with multiple-comparison post-hoc tests (ANOVA F=7.90, P<0.01). Specifically, CST-364S and CST-370L caused ~3.2- and ~2.6-times slower desensitization of the receptor than CST-WT. *P<0.05, **P<0.01 with respect to CST-WT.

consistent with the findings for the bovine CST peptide on oocytes (Herrero et al., 2002), suggesting a similar mode of action of the peptide across species on nAChRs. The greater blocking effect upon pre-equilibration suggests that the peptide must be present at its effective concentration during the entire activation phase of the receptor to exhibit its maximum effect. It is conceivable that the pre-equilibration of the receptor with the peptide might alter the activation and desensitization kinetics of the receptor. Indeed, a decrease in the activation rate ($\tau_{activation\text{-}CST\text{-}WT}$:$\tau_{activation\text{-}ACh}$= 1.4±0.09, i.e. ~40%) and an increase in the desensitization rate ($\tau_{Desensitization\text{-}CST\text{-}WT}$:$\tau_{Desensitization\text{-}ACh}$=0.12±0.02, i.e. ~88%) of the nAChR was observed in the presence of CST-WT (Fig. 7). Greater effect of CST upon pre-incubation might also result from state-dependent modulation of nAChRs; in the closed-state, binding sites might be fully accessible to the peptides, which is in agreement with our computational analysis. Another explanation for the enhanced blocking effect with pre-incubation of the peptide could be binding of CST to two sites: one high-affinity site at the pore of receptor and one low-affinity site located outside the channel; in the absence of pre-incubation, the peptide does not bind to the external site of the channel and hence display limited antagonistic effect (Herrero et al., 2002). However, our computational analysis did not favor a second binding site for CST outside the pore of the receptor. Additionally, the Hill coefficients for CST peptides for inhibition of nAChR activity (blockade of nicotine-evoked inward current; Fig 6D) were near unity (CST-WT, 0.98; CST-370L, 1.11; CST-364S, 0.96), arguing against the existence of more than one binding site for CST on the receptor.

Mechanistic basis of differential potencies of the human CST variants

Previously, we reported that IC_{50} values for inhibiting nicotine-evoked catecholamine release from un-differentiated PC12 cells for the CST variants were as follows: CST-370L (0.37 μM)<CST-WT (0.82 μM)<CST-364S (3.65 μM) (Mahapatra, 2008; Mahata et al., 2004). What might the mechanism be for such substantial (~tenfold) differences in the potency among these CST variants? Our computational analysis suggested that these peptides (1) differ in their conformational preferences for secondary structure, (2) bind with the nAChR with different affinities [the rank order of docking energy values being CST-370L<CST-WT<CST-364S], and (3) occlude the pore of the extracellular vestibule region of

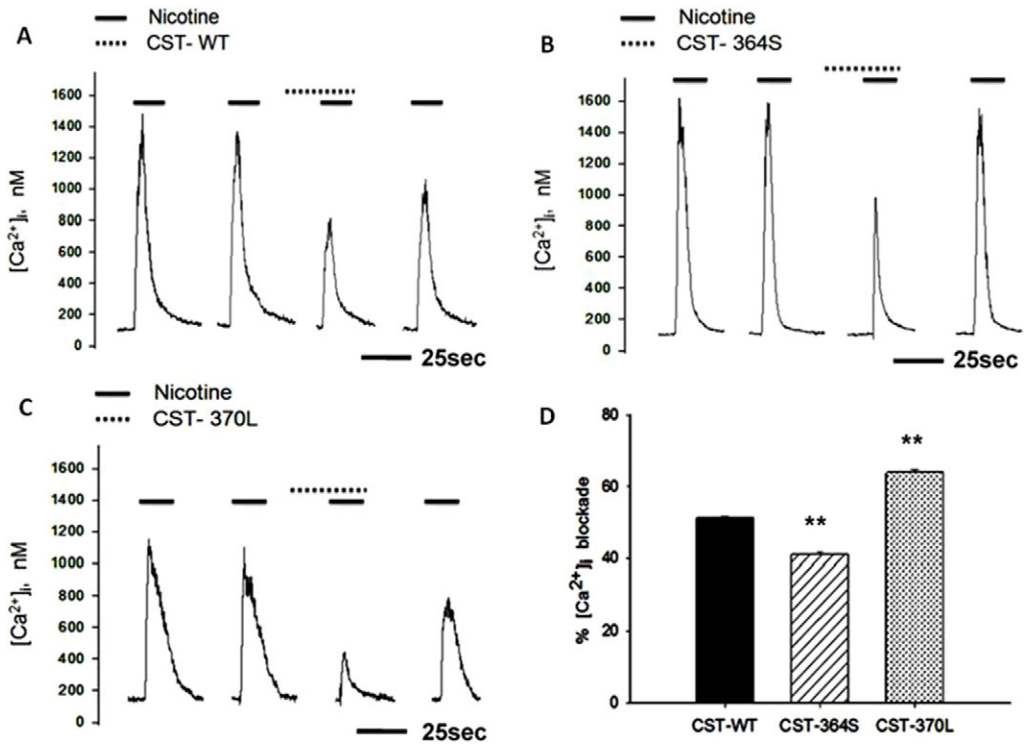

Fig. 8. Human CST peptides block nicotine-evoked elevation of intracellular free calcium concentration. NGF-differentiated PC12 cells loaded with Fura2-AM were stimulated with nicotine (200 μM) in the absence or presence of CST peptides (5 μM). The intracellular calcium concentration ($[Ca^{2+}]_i$) values were calculated from the Fura-2 fluorescence. (**A**–**C**) Representative $[Ca^{2+}]_i$ transients in the cases of CST-WT, CST-364S and CST-370L, respectively. The solid bars above the $[Ca^{2+}]_i$ traces indicate the applications of nicotine and the dotted bars indicate the applications of peptides in these experiments. (**D**) The percentage blockade of $[Ca^{2+}]_i$ for each CST peptide. Data plotted are mean ± s.e.m. values from 135 cells for CST-WT, 140 cells for CST-364S and 72 cells for CST-370L. One-way ANOVA, followed by post-hoc tests performed at 95% confidence interval between the groups suggested significant difference in blocking the nicotine-stimulated Ca^{2+} rises between the peptides. $^{**}P<0.01$ with respect to CST-WT.

the receptor to different extents such that the order of MPR values after peptide binding were: CST-370L<CST-WT<CST-364S (Fig. 5E). Consistent with these in silico results, the extent of inhibition of inward Na^+ currents in PC12 cells were in the following order: CST-370L>CST-WT>CST-364S (Fig. 6D). This observation corroborated with our previous finding that CST peptides blocked nicotine-induced $^{22}Na^+$ influx into un-differentiated PC12 cells in the same order (Mahata et al., 2004). Moreover, the blockade of Na^+ entry (as measured by inward current, Fig. 6) paralleled the blockade of catecholamine secretion (Fig. 9). In addition, the human CST variants blocked the entry of Ca^{2+} into the cytosol in the same order (Fig. 8), suggesting their specific inhibitory effect on nAChR signal transduction. The altered potencies of the peptides might also be accounted for by their effects on the kinetic parameters of nAChR activation and desensitization (Fig. 7). Taken together, structural variations in the CST peptide (specifically, the α-helical content) alter its binding affinity with nAChR, and thereby cause alterations in the extent of entry of Na^+ and Ca^{2+} into the cytosol, which, in turn, lead to differential inhibition of catecholamine release into the circulation (Fig. 10).

Conclusions and perspectives

Our multidisciplinary structure–function correlation approach revealed important molecular interactions of human CST with the human α3β4 receptor, a major nAChR subtype expressed in chromaffin cells and adrenergic neurons. Future studies might unravel whether human CST peptides also interact with additional human nAChR subtypes. This study also provided the mechanistic basis for differential activity (inhibition of nicotinic or cholinergic stimulus-evoked catecholamine secretion) of human CST variants. Of note, it has recently been reported that these CST variants display an analogous order of potency (CST-370L>CST-WT>CST-364S) to regulate infarct size in the regionally ischemic-reperfused rat heart, perhaps mediated through receptor(s) other than nAChRs (Brar et al., 2010). Therefore, it appears that the location of the variation in these CST peptides (and hence structural variations) might be crucial for their differential activities across their different receptors.

Because alterations in the catecholamine secretion have been associated with the pathogenesis of cardiovascular disease states such as hypertension (Esler et al., 2001; Goldstein, 1983; Guyenet, 2006; Joyner et al., 2010; Mathar et al., 2010; Rumantir et al., 2000) and catestatin acts a ‘physiological brake’ to inhibit neurotransmitters (e.g. catecholamines) release from chromaffin cells and noradrenergic neurons in mice as well as in humans, (Mahapatra et al., 2005; O’Connor et al., 2002), this study has implications for understanding the nicotinic cholinergic signaling and hence catecholamine physiology and pathophysiology in humans. Therefore, one can predict possible phenotypic associations of the genetic variations in the *CHGA*

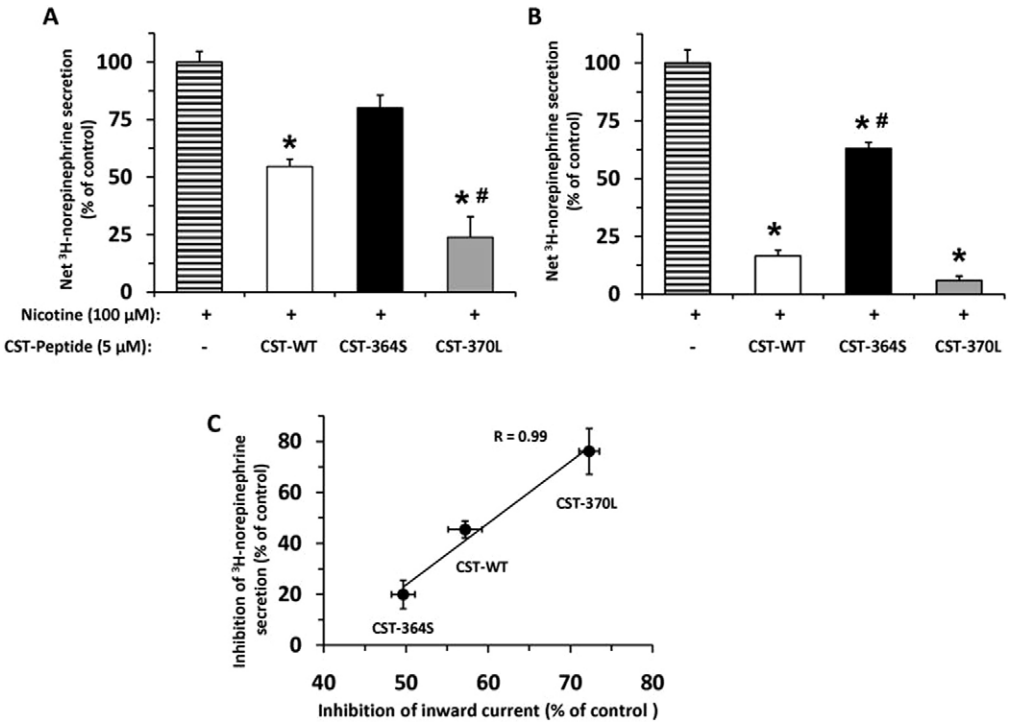

Fig. 9. Differential inhibition of catecholamine secretion by human CST-peptides and its positive correlation with inhibition of inward currents. NGF-differentiated (**A**) and un-differentiated (**B**) PC12 cells were loaded with [^{3}H]norepinephrine and stimulated with nicotinic cholinergic agonist (100 µM nicotine) in the absence or presence of human CST peptides (5 µM). The inhibition of net [^{3}H]norepinephrine secretion by each peptide was expressed as a percentage of control and the values are plotted as mean ± s.e.m. of three separate wells. Control (100%) net [^{3}H]norepinephrine secretion was that in the presence of nicotine alone, without any CST peptide. The CST peptides displayed significant differences in activity in both NGF-differentiated (one-way ANOVA $F=31.8$; $^*P<0.001$ with respect to the control, $^{\#}P<0.05$ with respect to the CST-WT) and undifferentiated (one-way ANOVA $F=81.9$; $^*P<0.001$ with respect to the control, $^{\#}P<0.05$ with respect to the CST-WT). (**C**) Parallel batches of NGF-treated PC12 cells were assessed for the inhibitory effect of each CST peptide (5 µM) on nicotine (100 µM)-stimulated catecholamine ([^{3}H]norepinephrine) secretion and acetylcholine (100 µM)-evoked inward currents. A strong positive correlation ($y=2.422x–97.45$; $R=0.99$) between percentage inhibition of catecholamine secretion and percentage inhibition of inward currents was observed.

gene leading to these naturally occurring CST variants. Indeed, the Gly364Ser variation has been strongly associated with profound changes in cardiac activity, alterations in renal or plasma catecholamine secretion, blood pressure variation and prediction of risk for essential hypertension in a European population (Rao et al., 2007).

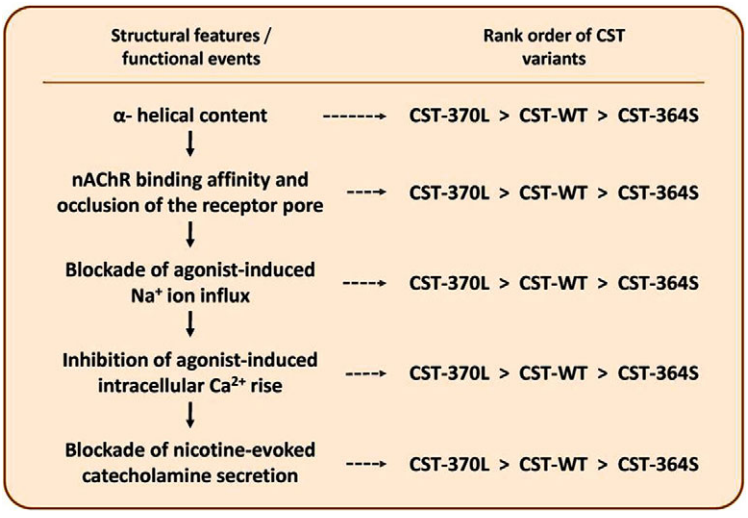

Fig. 10. Molecular basis for differential activities of the human CST peptides: a schematic presentation. Structural variations among the CST peptides (specifically, the α-helical content) govern their binding affinity with nAChR as well as the extent of occlusion of the receptor pore. Such differential interactions of the CST peptides with the receptor alter the extents of influx of Na^+ and Ca^{2+} into the cytosol, which in turn lead to differential inhibition of catecholamine release evoked by nicotinic cholinergic agonist. At each stage of the neuronal nicotinic signal transduction pathway, the CST peptides displayed parallel rank order of activities (CST-370L>CST-WT>CST-364S).

Materials and Methods

Building the structure of the human α3β4 nAChR

A homology-modeled closed-channel structure of the human $(\alpha3)_2(\beta4)_3$ nAChR was built using Modeller (9v7; http://salilab.org/modeller/) (Sali and Blundell, 1993) based on the 4.0 Å resolution structure of *Torpedo marmorata* nAChR (PDB ID: 2BG9) (Unwin, 2005). We used the similar strategy that was recently used to model the human $(\alpha4)_2(\beta2)_3$ nAChR (Haddadian et al., 2008). In brief, sequences of the human α3 (P32297) and β4 (P30926) subunits were obtained from the SwissProt protein knowledgebase at the Expasy Server (http://www.expasy.ch/sprot). Modeling human α3 and β4 subunits was carried out using α and β subunits of the *Torpedo* receptor, respectively. The residues connecting the third TM helix with the IC helix in each subunit were not modeled because of the absence of suitable template. A set of 20 models was generated for the human α3 and β4 subunits. These models were then evaluated based on Discrete Optimized Protein Energy (DOPE) values and the best models (i.e., with lowest energy values) were selected for building the pentameric model. Two α3 and three β4 subunits were superimposed onto the *Torpedo* nAChR structure in the order α3:α β4:γ α3:α β4:δ β4:β and energy minimized using Swiss PDB Viewer (Guex and Peitsch, 1997) to generate the pentameric human $(\alpha3)_2(\beta4)_3$ nAChR with 1852 residues forming the ligand binding extracellular (EC), TM and IC domains. Quality of the model was evaluated by using the PROCHECK program (Laskowski et al., 1993).

Generation of the structures of human wild-type and variant catestatin peptides

NMR-determined structure of human wild-type catestatin (CST-WT) (PDB ID: 1LV4) (Preece et al., 2004) was taken, equilibrated in water at 300 K and 1 atm pressure using AMBER force field (Simmerling et al., 2002) in NAMD2.6 package (Phillips et al., 2005) for about 10 nanoseconds. Models of the naturally occurring variants of CST (CST-364S, CST-370L) were obtained by introducing the respective mutations using the mutagenesis wizard in PyMOL (The PyMOL Molecular Graphics System, version 1.3, Schrödinger, LLC). The same equilibration procedure as mentioned above for the CST-WT was followed to equilibrate the structures of CST-364S, CST-370L peptides. These three peptides were then simulated for 170 nanoseconds in water and the final structures from simulation were considered for further studies. The resultant structures were analyzed in Visual Molecular Dynamics (VMD) software (Humphrey et al., 1996) using home-built codes.

Generation and simulation of the membrane–nAChR complex

A membrane (dimensions: 120 Å × 120 Å) comprising of 1-palmitoyl-2-oleoyl–*sn*-glycerol–phospatidyl choline (POPC) was generated in VMD using the Membrane Builder plug-in. The lipids 1-palmitoyl-2-oleoyl-sn-glycerol phosphatidic acid (POPA) and cholesterol (CHOL) were then added into the membrane such that the final ratio of POPC:POPA:CHOL was 3:1:1. This particular stoichiometry of the lipid molecules were chosen based on previous reports (Brannigan et al., 2008; Cheng et al., 2007; daCosta et al., 2002). The membrane was then further equilibrated to induce the appropriate disorder of a fluid-like bilayer. The structure and thickness of the generated bilayer were validated from the plot of mass density along the normal to the plane of the bilayer (supplementary material Fig. S5).

The EC and TM domains of the modeled structure of the human α3β4 nAChR (Fig. 1A,B) was embedded into the equilibrated membrane and extra water molecules were added to completely solvate the EC ligand-binding domain. The IC domain was avoided in this process for reduction of computational cost. Charge neutralization was then done by adding 79 Na^+ ions. The final system was comprised of 196 POPC lipids, 64 POPA, 71 cholesterol (~3:1:1), 42,597 water molecules, 79 Na^+ ions and 1 human $\alpha_3\beta_4$ nAChR, making up a total of 194,714 atoms. This receptor–membrane complex was energy-minimized and subsequently, the imposed restraints on heavy atoms of the protein were taken off during the initial 4 nanoseconds of MD simulation. The system was then equilibrated for 80 nanoseconds at 300 K and 1 atm using the NAMD2.6 package (Phillips et al., 2005).

Docking of ligands (CST peptides) onto the equilibrated nAChR receptor

Docking of CST-WT, CST-364S and CST-370L peptides on the extracellular domain of nAChR was performed using Autodock 3.05 (Morris et al., 1998). A 200 × 200 × 180 Å grid box at the center of the exoplasmic domain of the receptor with 0.375 Å spacing was used to search the ligand binding region. The Lamarckian genetic algorithm (LGA) with a population size of 300 and number of energy evaluations as 25 million was used. The receptor and the CST peptide were rigid during docking. 500 LGA runs were carried out, followed by clustering of the ligand conformations with an RMSD cut-off of 0.5 Å. The lowest energy conformation of the ligand from each cluster was selected, a separate co-ordinate file in the PDB format was generated for the receptor–ligand complex by catenating their co-ordinates and visually compared using the VMD program.

Post-docking molecular dynamics simulations

The peptide–receptor complex generated after docking was embedded in the membrane bilayer and simulated at 300 K and 1 atm pressure using the NAMD2.6 package in order to introduce flexibility in the ligand. Final simulated complexes were then picked for various analyses. The peptide receptor interactions for the three peptides were calculated using the protein interactions calculator (PIC) webserver (Tina et al., 2007) using the default cut-offs for the different type of interactions: hydrophobic, ionic, hydrogen bonding and aromatic group interactions. Interaction energy of the stable, bound peptide after achieving flexibility in MD simulations was evaluated using Autodock 3.05 energy-scoring function. The percentage occlusion of the pore was calculated by using HOLE (Smart et al., 1993) software with default parameters.

Circular dichroism spectroscopic analysis of CST peptides

CST peptides (synthesized and purified to >95% homogeneity by Genpro Biotech, New Delhi, India) were dissolved in water at a concentration of 5 mM. For CD spectroscopy, the stock solutions were diluted to 100 µM final concentration in phosphate-buffered saline (PBS), pH 7.4. To study trifluoroethanol (TFE)-induced secondary structure formation, TFE was added to the stock peptide solution such that the peptide concentration became 100 µM and the final TFE concentrations (v/v) were 10%, 30%, 60% and 90% in PBS. An aliquot (200 µl) of each of these samples (without or with TFE) was placed into a 0.1 cm path-length quartz cell (Hellma, Forest Hills, NY) and CD measurements were performed using a JASCO Spectropolarimeter (model J-810). All measurements were done at 25°C. Spectra were recorded over the wavelength range of 198–260 nm. Three individual experiments were carried out for each sample. Raw data were calibrated by smoothing and subtraction of buffer spectra, according to the manufacturer's instructions.

Spectral deconvolution of CD data was performed using the CDPro software package (http://lamar.colostate.edu/~sreeram/CDPro/main.html), which consisted of three programs (SELCON3, CDSSTR and CONTIN LL) to determine relative quantities of random coil, α-helix, β-sheet and β-turn. In the CDPro package, reference sets of proteins from different sources are combined to create a large reference set of CD spectra and depending upon the spectrum wavelength range of the experiment, the reference set (IBasis) can be changed. We used an IBasis of 7, which contained 48 proteins reference set and wavelength range of 198 to 240 nm for our calculations. Deconvolution was done with each of the three programs. If the data obtained were similar from the three different programs, they were averaged to obtain the percentage of each secondary structure element. In some cases, the results obtained from one program were not convergent with those from the other two. In such cases, averaging was done only with the data from two other programs. For example, at 0% TFE, convergent solutions were not obtained using SELCON3 program. Therefore, in these cases, the data obtained from SELCON3 were excluded in the calculation. For comparison and more confidence on our data, deconvolution was also performed using CDANAL software (Perczel et al., 1992). Brahms and Brahms reference library was used for CDANAL deconvolution. Both methods gave comparable results; however, we have included only the CDPro-deconvoluted data in this study.

Cell culture conditions

Rat pheochromocytoma PC12 cells, obtained from the National Centre for Cell Sciences, Pune, India were used in all experiments. For routine maintenance, cells were grown in 8.8 cm square dishes (Nunc) in Dulbecco's modified Eagle's high-glucose medium (DMEM) supplemented with 10% heat-inactivated horse serum, 5% heat-inactivated fetal bovine serum, 100 U/ml penicillin G and 100 µg/ml streptomycin (Gibco) at 37°C and 5.5% CO_2 in a humidified incubator (Thermo Scientific). Cells were passaged every 4 to 5 days or when confluent. To carry out various experiments (detailed below), cells were seeded on poly-L-lysine-coated six-well plates (Nunc) or coverslips in 35 mm polypropylene Petri dishes (Nunc). For neuronal differentiation, PC12 cells were treated with 100 ng/ml of NGF (Sigma) and the medium was changed after 24 hours. Fresh medium with NGF was added and cells were grown for two more days and experiments on the NGF-differentiated cells were carried out on the fourth day (after seeding).

Electrophysiology (patch-clamp) experiments

NGF-treated PC12 cells grown on poly-L-lysine-coated glass coverslips (11 mm diameter; Hi-Media) were transferred to a recording chamber (RC-26G, Warner Instruments) mounted on the stage of an Olympus IX71 inverted microscope attached with ANDOR CCD camera. The chamber was continuously perfused at 5–8 ml/minute with an extracellular solution containing 150 mM NaCl, 5 mM KCl, 1 mM $CaCl_2$, 1 mM $MgCl_2$, 5 mM glucose, 5 mM HEPES, pH 7.4. Patch pipettes having resistances of 4–7 MΩ, pulled with P-97 micropipette Puller (Sutter Instrument Company), contained 140 mM CsCl, 2 mM $MgCl_2$, 0.2 mM $CaCl_2$, 1.1 mM EGTA, 10 mM HEPES, pH 7.4. A conventional whole-cell patch-clamp method was used to measure the acetylcholine (ACh)-induced currents in cells clamped at −80 mV, with the help of Axopatch 200B amplifier (Molecular Devices) at room temperature (22–24°C). Current traces were low-pass filtered at 5 KHz and digitized at 15 KHz with the help of Digidata 1440A (Molecular

Devices). Data acquisition and analysis were carried out with Pclamp 10 software (Molecular Devices).

Currents were elicited by brief applications (~3 seconds) of ACh (acetylcholine chloride, 100 μM; Sigma). For measuring desensitization kinetics, the duration of ACh application was prolonged to 40–60 seconds. Two consecutive pulses of ACh separated by at least 2 minutes of wash were given to check the rundown of the currents. To monitor the effect of wild-type CST (CST-WT) and its variants (CST-360S and CST-370L), cells were incubated with the peptides for 2 minutes, followed by a pulse of ACh with the peptide. Cells showing no run-down in current amplitudes were considered for treatment with the CST peptides. To determine the potencies (as IC_{50} for each CST peptide that elicits the half-maximal of inward current), experiments were carried out with several doses of the peptide (100 nM, 250 nM, 1 μM, 2.5 μM, 5 μM and 10 μM). Efficacies of the peptides were determined as percentage inhibition of the inward current at 5 μM and 10 μM peptide doses. Experiments were carried out at three different times and $n=7$ cells were considered for data analysis. SigmaPlot version 11.0 (Systat Software) was used for data fitting. The IC_{50} values and Hill coefficients for different peptides were calculated by non-linear regression wizard with a three-parameter logistic equation. The activation and desensitization time constants ($\tau_{activation}$ and $\tau_{desensitization}$) were determined by fitting the current traces with standard exponential function with single parameter, using Pclamp 10 software (Molecular Devices). The graphs were plotted for the ratio $\tau_{peptide}$:τ_{ACh} both for activation and desensitization. For example, in the case of the activation graph, the plot was generated using $\tau_{activation(peptide)}$:$\tau_{activation(ACh)}$ values. Similarly, the desensitization plot was generated using $\tau_{desensitization(peptide)}$:$\tau_{desensitization(ACh)}$ values.

Measurement of intracellular calcium concentrations

$[Ca^{2+}]_i$ was measured by a ratiometric method using Fura 2-AM dye (Invitrogen). In brief, NGF-treated PC12 cells grown on coverslips were incubated with 5 μM Fura 2-AM (Invitrogen) in bathing solution (120 mM NaCl, 5 mM KCl, 5 mM $CaCl_2$, 2 mM $MgCl_2$, 10 mM glucose, 10 mM HEPES, pH 7.4) at room temperature (22–24℃) for 30 minutes, followed by washing with the bathing solution for 30 minutes. Cells were illuminated with dual-excitation wavelengths (at 340 nm and 380 nm) and emission was captured at 510 nm with appropriate excitation and emission filters. Images were acquired by an Andor CCD camera attached with Olympus IX71, controlled through Andor iQ software (Andor Technology).

Nicotine-induced Ca^{2+} rise was measured by applying 200 μM of nicotine bitartarate (Sigma) in bathing solution. To see the effect of CST peptides, cells were pre-incubated with 5 μM of a peptide for 2 minutes, followed by its co-application with nicotine. $[Ca^{2+}]_i$ rise in the presence of each peptide was compared with the corresponding control (basal level). Regions of interest were drawn to define borders of cells and fluorescence ratios (340 nm/380 nm) were calculated from the background subtracted images. The apparent $[Ca^{2+}]_i$ concentration was derived by using the equation: $[Ca^{2+}]_i = K_d(R-R_{min})/(R_{max}-R)\beta$ (Grynkiewicz et al., 1985), where K_d was the dissociation constant of Fura-2-Ca^{2+} complex, R was the emission ratio of fluorescent intensities at 340 and 380 nm (F_{340}/F_{380}), R_{min} and R_{max} were the emission ratio of F_{340}/F_{380} at zero calcium (i.e. in the presence of 0 mM $CaCl_2$ plus 3 μM ionomycin [Sigma]) and saturated calcium (i.e. in the presence 10 mM $CaCl_2$ plus 3 μM ionomycin) levels respectively, β (=8.2) was the ratio of Fura-2 fluorescence at 380 nm, in the free state (zero calcium) to the bound state (saturated calcium condition). For measuring R_{min}, Fura-2 loaded cells were first incubated in calcium-free bath solution containing 5 mM EGTA for 15–20 min, followed by the application of same solution supplemented with 3 μM ionomycin for 2–3 minutes. R_{max} was measured after incubating the cells in bath solution containing 3 μM ionomycin and 10 mM $CaCl_2$ for 3–5 minutes. The R_{min} and R_{max} values were 0.73 and 12.8, respectively. The K_d value was taken as 274 nM as per previous reports (Reber et al., 1993; Shuttleworth and Thompson, 1991). Statistical analysis was carried out using the data from $n=135$ cells for CST-WT, $n=140$ cells for CST-364S and $n=72$ cells for CST-370L peptides, generated from at least three independent experiments.

Catecholamine secretion experiments

Catecholamine secretion was assayed as described previously (Mahapatra et al., 2006) with slight modifications. In brief, undifferentiated or NGF-differentiated PC12 cells grown in six-well plates and labeled with 0.5 μCi of L-[7-^{3}H]norepinephrine (PerkinElmer) for 2 hours at 37℃ were washed once for 2 minutes with release buffer (150 mM NaCl, 5 mM KCl, 2 mM $CaCl_2$, 10 mM HEPES, pH 7) and once (for 20 minutes) with DMEM, and incubated for 20 minutes at 37℃ in release buffer with or without nicotine (100 μM). Supernatant was collected 20 minutes after treatment, and then cells were lysed in lysis buffer [150 mM NaCl, 5 mM KCl, 2mM $CaCl_2$, 10 mM HEPES, pH 7, 0.1% (v/v) Triton X-100]. Secretion media and cell lysates were assayed for [^{3}H]norepinephrine counts by using a PerkinElmer Tricarb liquid scintillation counter and results were expressed as percentage secretion: (amount released/[amount released + amount in cell lysate]) × 100. Net secretion was calculated as stimulated release minus basal or unstimulated release of catecholamines.

Data presentation and statistical analysis

The experimental data presented in this report are representatives of three to five separate experiments. Results are expressed as mean ± s.e.m. values from replicate cells or wells as indicated in the respective figure legends. One-way ANOVA and Post-hoc tests (Gabriel, Hochberg and Games–Howell) were performed at 95% confidence interval using SPSS. $P \leq 0.05$ was chosen for statistical significance between the groups.

Funding

This study was supported by grants from the Department of Biotechnology [grant numbers BT/PR12820/BRB/10/726/2009 to N.R.M. and S.S.]; and the Department of Science and Technology [grant number SR/SO/BB-47/2008 to N.R.M. and A.K.B.] of the Government of India.

Supplementary material available online at
http://jcs.biologists.org/lookup/suppl/doi:10.1242/jcs.103176/-/DC1

References

Avila, A. M., Dávila-García, M. I., Ascarrunz, V. S., Xiao, Y. and Kellar, K. J. (2003). Differential regulation of nicotinic acetylcholine receptors in PC12 cells by nicotine and nerve growth factor. *Mol. Pharmacol.* **64**, 974-986.

Barrantes, F. J. (2004). Structural basis for lipid modulation of nicotinic acetylcholine receptor function. *Brain Res. Brain Res. Rev.* **47**, 71-95.

Biswas, N., Rodriguez-Flores, J. L., Courel, M., Gayen, J. R., Vaingankar, S. M., Mahata, M., Torpey, J. W., Taupenot, L., O'Connor, D. T. and Mahata, S. K. (2009). Cathepsin L colocalizes with chromogranin a in chromaffin vesicles to generate active peptides. *Endocrinology* **150**, 3547-3557.

Bond, C. S. and Schüttelkopf, A. W. (2009). ALINE: a WYSIWYG protein-sequence alignment editor for publication-quality alignments. *Acta Crystallogr. D Biol. Crystallogr.* **65**, 510-512.

Brannigan, G., Hénin, J., Law, R., Eckenhoff, R. and Klein, M. L. (2008). Embedded cholesterol in the nicotinic acetylcholine receptor. *Proc. Natl. Acad. Sci. USA* **105**, 14418-14423.

Brar, B. K., Helgeland, E., Mahata, S. K., Zhang, K., O'Connor, D. T., Helle, K. B. and Jonassen, A. K. (2010). Human catestatin peptides differentially regulate infarct size in the ischemic-reperfused rat heart. *Regul. Pept.* **165**, 63-70.

Cheng, M. H., Liu, L. T., Saladino, A. C., Xu, Y. and Tang, P. (2007). Molecular dynamics simulations of ternary membrane mixture: phosphatidylcholine, phosphatidic acid, and cholesterol. *J. Phys. Chem. B* **111**, 14186-14192.

daCosta, C. J. B., Ogrel, A. A., McCardy, E. A., Blanton, M. P. and Baenziger, J. E. (2002). Lipid-protein interactions at the nicotinic acetylcholine receptor. A functional coupling between nicotinic receptors and phosphatidic acid-containing lipid bilayers. *J. Biol. Chem.* **277**, 201-208.

Esler, M., Rumantir, M., Kaye, D., Jennings, G., Hastings, J., Socratous, F. and Lambert, G. (2001). Sympathetic nerve biology in essential hypertension. *Clin. Exp. Pharmacol. Physiol.* **28**, 986-989.

Friese, R. S., Mahboubi, P., Mahapatra, N. R., Mahata, S. K., Schork, N. J., Schmid-Schönbein, G. W. and O'Connor, D. T. (2005). Common genetic mechanisms of blood pressure elevation in two independent rodent models of human essential hypertension. *Am. J. Hypertens.* **18**, 633-652.

Fung, M. M., Salem, R. M., Mehtani, P., Thomas, B., Lu, C. F., Perez, B., Rao, F., Stridsberg, M., Ziegler, M. G., Mahata, S. K. et al. (2010). Direct vasoactive effects of the chromogranin A (CHGA) peptide catestatin in humans *in vivo*. *Clin. Exp. Hypertens.* **32**, 278-287.

Goldstein, D. S. (1983). Plasma catecholamines and essential hypertension. An analytical review. *Hypertension* **5**, 86-99.

Grynkiewicz, G., Poenie, M. and Tsien, R. Y. (1985). A new generation of Ca^{2+} indicators with greatly improved fluorescence properties. *J. Biol. Chem.* **260**, 3440-3450.

Guex, N. and Peitsch, M. C. (1997). SWISS-MODEL and the Swiss-PdbViewer: an environment for comparative protein modeling. *Electrophoresis* **18**, 2714-2723.

Guyenet, P. G. (2006). The sympathetic control of blood pressure. *Nat. Rev. Neurosci.* **7**, 335-346.

Haddadian, E. J., Cheng, M. H., Coalson, R. D., Xu, Y. and Tang, P. (2008). In silico models for the human alpha4beta2 nicotinic acetylcholine receptor. *J. Phys. Chem. B* **112**, 13981-13990.

Helle, K. B. (2010). Regulatory peptides from chromogranin A and secretogranin II. *Cell. Mol. Neurobiol.* **30**, 1145-1146.

Henderson, L. P., Gdovin, M. J., Liu, C., Gardner, P. D. and Maue, R. A. (1994). Nerve growth factor increases nicotinic ACh receptor gene expression and current density in wild-type and protein kinase A-deficient PC12 cells. *J. Neurosci.* **14**, 1153-1163.

Herrero, C. J., Alés, E., Pintado, A. J., López, M. G., García-Palomero, E., Mahata, S. K., O'Connor, D. T., García, A. G. and Montiel, C. (2002). Modulatory mechanism of the endogenous peptide catestatin on neuronal nicotinic acetylcholine receptors and exocytosis. *J. Neurosci.* **22**, 377-388.

Humphrey, W., Dalke, A. and Schulten, K. (1996). VMD: visual molecular dynamics. *J. Mol. Graph.* **14**, 33-38, 27-28.

Joyner, M. J., Charkoudian, N. and Wallin, B. G. (2010). Sympathetic nervous system and blood pressure in humans: individualized patterns of regulation and their implications. *Hypertension* **56**, 10-16.

Laskowski, R. A., MacArthur, M. W., Moss, D. S. and Thornton, J. M. (1993). PROCHECK: a program to check the stereochemical quality of protein structures. *J. Appl. Cryst.* **26**, 283-291.

Law, R. J., Henchman, R. H. and McCammon, J. A. (2005). A gating mechanism proposed from a simulation of a human alpha7 nicotinic acetylcholine receptor. *Proc. Natl. Acad. Sci. USA* **102**, 6813-6818.

Mahapatra, N. R. (2008). Catestatin is a novel endogenous peptide that regulates cardiac function and blood pressure. *Cardiovasc. Res.* **80**, 330-338.

Mahapatra, N. R., O'Connor, D. T., Vaingankar, S. M., Hikim, A. P., Mahata, M., Ray, S., Staite, E., Wu, H., Gu, Y., Dalton, N. et al. (2005). Hypertension from targeted ablation of chromogranin A can be rescued by the human ortholog. *J. Clin. Invest.* **115**, 1942-1952.

Mahapatra, N. R., Mahata, M., Mahata, S. K. and O'Connor, D. T. (2006). The chromogranin A fragment catestatin: specificity, potency and mechanism to inhibit exocytotic secretion of multiple catecholamine storage vesicle co-transmitters. *J. Hypertens.* **24**, 895-904.

Mahata, S. K., O'Connor, D. T., Mahata, M., Yoo, S. H., Taupenot, L., Wu, H., Gill, B. M. and Parmer, R. J. (1997). Novel autocrine feedback control of catecholamine release. A discrete chromogranin a fragment is a noncompetitive nicotinic cholinergic antagonist. *J. Clin. Invest.* **100**, 1623-1633.

Mahata, S. K., Mahata, M., Wakade, A. R. and O'Connor, D. T. (2000). Primary structure and function of the catecholamine release inhibitory peptide catestatin (chromogranin A(344-364)): identification of amino acid residues crucial for activity. *Mol. Endocrinol.* **14**, 1525-1535.

Mahata, S. K., Mahata, M., Wen, G., Wong, W. B., Mahapatra, N. R., Hamilton, B. A. and O'Connor, D. T. (2004). The catecholamine release-inhibitory "catestatin" fragment of chromogranin a: naturally occurring human variants with different potencies for multiple chromaffin cell nicotinic cholinergic responses. *Mol. Pharmacol.* **66**, 1180-1191.

Mathar, I., Vennekens, R., Meissner, M., Kees, F., Van der Mieren, G., Camacho Londoño, J. E., Uhl, S., Voets, T., Hummel, B., van den Bergh, A. et al. (2010). Increased catecholamine secretion contributes to hypertension in TRPM4-deficient mice. *J. Clin. Invest.* **120**, 3267-3279.

Morris, G. M., Goodsell, D. S., Halliday, R. S., Huey, R., Hart, W. E., Belew, R. K. and Olson, A. J. (1998). Automated docking using a Lamarckian genetic algorithm and an empirical binding free energy function. *J. Comput. Chem.* **19**, 1639-1662.

Nery, A. A., Resende, R. R., Martins, A. H., Trujillo, C. A., Eterovic, V. A. and Ulrich, H. (2010). Alpha 7 nicotinic acetylcholine receptor expression and activity during neuronal differentiation of PC12 pheochromocytoma cells. *J. Mol. Neurosci.* **41**, 329-339.

O'Connor, D. T., Takiyyuddin, M. A., Printz, M. P., Dinh, T. Q., Barbosa, J. A., Rozansky, D. J., Mahata, S. K., Wu, H., Kennedy, B. P., Ziegler, M. G. et al. (1999). Catecholamine storage vesicle protein expression in genetic hypertension. *Blood Press.* **8**, 285-295.

O'Connor, D. T., Kailasam, M. T., Kennedy, B. P., Ziegler, M. G., Yanaihara, N. and Parmer, R. J. (2002). Early decline in the catecholamine release-inhibitory peptide catestatin in humans at genetic risk of hypertension. *J. Hypertens.* **20**, 1335-1345.

Perczel, A., Park, K. and Fasman, G. D. (1992). Analysis of the circular dichroism spectrum of proteins using the convex constraint algorithm: a practical guide. *Anal. Biochem.* **203**, 83-93.

Phillips, J. C., Braun, R., Wang, W., Gumbart, J., Tajkhorshid, E., Villa, E., Chipot, C., Skeel, R. D., Kalé, L. and Schulten, K. (2005). Scalable molecular dynamics with NAMD. *J. Comput. Chem.* **26**, 1781-1802.

Preece, N. E., Nguyen, M., Mahata, M., Mahata, S. K., Mahapatra, N. R., Tsigelny, I. and O'Connor, D. T. (2004). Conformational preferences and activities of peptides from the catecholamine release-inhibitory (catestatin) region of chromogranin A. *Regul. Pept.* **118**, 75-87.

Rana, B. K., Wessel, J., Mahboubi, V., Rao, F., Haeller, J., Gayen, J. R., Eskin, E., Valle, A. M., Das, M., Mahata, S. K. et al. (2009). Natural variation within the neuronal nicotinic acetylcholine receptor cluster on human chromosome 15q24: influence on heritable autonomic traits in twin pairs. *J. Pharmacol. Exp. Ther.* **331**, 419-428.

Rao, F., Wen, G., Gayen, J. R., Das, M., Vaingankar, S. M., Rana, B. K., Mahata, M., Kennedy, B. P., Salem, R. M., Stridsberg, M. et al. (2007). Catecholamine release-inhibitory peptide catestatin (chromogranin A(352-372)): naturally occurring amino acid variant Gly364Ser causes profound changes in human autonomic activity and alters risk for hypertension. *Circulation* **115**, 2271-2281.

Reber, B. F., Stucki, J. W. and Reuter, H. (1993). Unidirectional interaction between two intracellular calcium stores in rat phaeochromocytoma (PC12) cells. *J. Physiol.* **468**, 711-727.

Rezvani, K., Teng, Y. and De Biasi, M. (2010). The ubiquitin-proteasome system regulates the stability of neuronal nicotinic acetylcholine receptors. *J. Mol. Neurosci.* **40**, 177-184.

Rice, P., Longden, I. and Bleasby, A. (2000). EMBOSS: The European molecular biology open software suite. *Trends Genet.* **16**, 276-277.

Rumantir, M. S., Jennings, G. L., Lambert, G. W., Kaye, D. M., Seals, D. R. and Esler, M. D. (2000). The 'adrenaline hypothesis' of hypertension revisited: evidence for adrenaline release from the heart of patients with essential hypertension. *J. Hypertens.* **18**, 717-723.

Sahu, B. S., Sonawane, P. J. and Mahapatra, N. R. (2010). Chromogranin A: a novel susceptibility gene for essential hypertension. *Cell. Mol. Life Sci.* **67**, 861-874.

Sala, F., Nistri, A. and Criado, M. (2008). Nicotinic acetylcholine receptors of adrenal chromaffin cells. *Acta Physiol. (Oxf.)* **192**, 203-212.

Sali, A. and Blundell, T. L. (1993). Comparative protein modelling by satisfaction of spatial restraints. *J. Mol. Biol.* **234**, 779-815.

Shuttleworth, T. J. and Thompson, J. L. (1991). Effect of temperature on receptor-activated changes in $[Ca^{2+}]$i and their determination using fluorescent probes. *J. Biol. Chem.* **266**, 1410-1414.

Simmerling, C., Strockbine, B. and Roitberg, A. E. (2002). All-atom structure prediction and folding simulations of a stable protein. *J. Am. Chem. Soc.* **124**, 11258-11259.

Smart, O. S., Goodfellow, J. M. and Wallace, B. A. (1993). The pore dimensions of gramicidin A. *Biophys. J.* **65**, 2455-2460.

Sönnichsen, F. D., Van Eyk, J. E., Hodges, R. S. and Sykes, B. D. (1992). Effect of trifluoroethanol on protein secondary structure: an NMR and CD study using a synthetic actin peptide. *Biochemistry* **31**, 8790-8798.

Sugawara, M., Resende, J. M., Moraes, C. M., Marquette, A., Chich, J.-F., Metz-Boutigue, M. H. and Bechinger, B. (2010). Membrane structure and interactions of human catestatin by multidimensional solution and solid-state NMR spectroscopy. *FASEB J.* **24**, 1737-1746.

Takiyyuddin, M. A., Parmer, R. J., Kailasam, M. T., Cervenka, J. H., Kennedy, B., Ziegler, M. G., Lin, M.-C., Li, J., Grim, C. E., Wright, F. A. et al. (1995). Chromogranin A in human hypertension. Influence of heredity. *Hypertension* **26**, 213-220.

Taupenot, L., Harper, K. L. and O'Connor, D. T. (2003). The chromogranin-secretogranin family. *N. Engl. J. Med.* **348**, 1134-1149.

Tina, K. G., Bhadra, R. and Srinivasan, N. (2007). PIC: protein interactions calculator. *Nucleic Acids Res.* **35**, W473-W476.

Tsigelny, I., Mahata, S. K., Taupenot, L., Preece, N. E., Mahata, M., Khan, I., Parmer, R. J. and O'Connor, D. T. (1998). Mechanism of action of chromogranin A on catecholamine release: molecular modeling of the catestatin region reveals a beta-strand/loop/beta-strand structure secured by hydrophobic interactions and predictive of activity. *Regul. Pept.* **77**, 43-53.

Unwin, N. (2005). Refined structure of the nicotinic acetylcholine receptor at 4A resolution. *J. Mol. Biol.* **346**, 967-989.

Wen, G., Mahata, S. K., Cadman, P., Mahata, M., Ghosh, S., Mahapatra, N. R., Rao, F., Stridsberg, M., Smith, D. W., Mahboubi, P. et al. (2004). Both rare and common polymorphisms contribute functional variation at CHGA, a regulator of catecholamine physiology. *Am. J. Hum. Genet.* **74**, 197-207.